Large FoV millimetre camera for high angular resolution sky mapping at 30m IRAM telescope

NIKA2

SAPIENZA UNIVERSITÀ DI ROMA

Marco De Petris

PhD Astronomy, Astrophysics and Space Science

November 30th, 2021 – Tor Vergata University in Rome

AASS PhD lesson on NIKA2

(New IRAM KID Arrays 2)

I. **Scientific questions/goals of NIKA2**
   - ✓ 5 main topics in 5 Large Programs on GT (+ OT targets)

II. **Focus on clusters of galaxies science by Sunyaev-Zel'dovich effect**
   - ✓ 1 LP on SZ to exploit P(r) *vs* z and Y *vs* M scaling law

III. **NIKA2 instrument description and observational operations**
   - ✓ mm-kilopixel camera at 150GHz and 260GHz bands with intensity and polarization capabilities

IV. **Scientific results and on-going observations**
   - ✓ High resolution mm-observations of high redshift clusters

V. **Hydrodynamical sims to support NIKA2 clusters science**
   - ✓ MUSIC and The Three Hundred projects

5 **Large Programs** on Guaranteed (*observational*) Time (1300h)
all of them linked to millimetre high angular resolution
and fast sky mapping of NIKA2

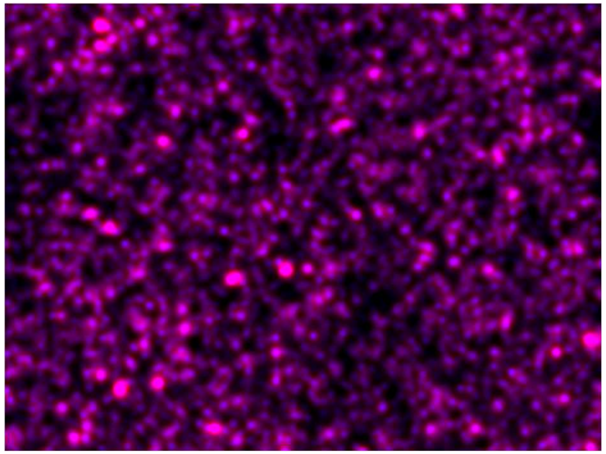

Deep Surveys
Mapping large sky areas at a depth close to the confusion limit to detect hundreds of dust-obscured optically-faint galaxies during their major episodes of formation in the early universe;

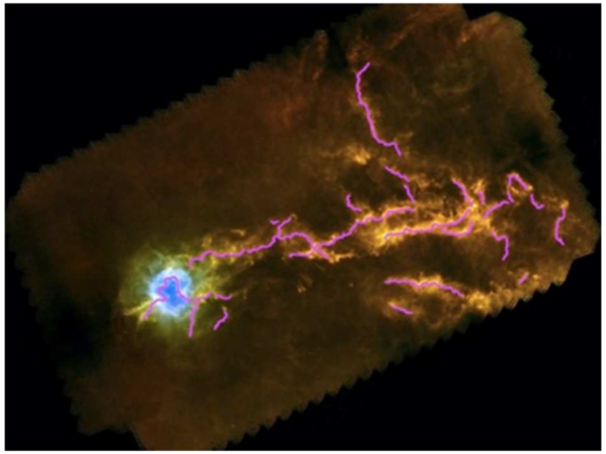

Mapping the InsterStellar Medium
A unique opportunity both to constrain dust properties in the millimeter wavelength domain, and to provide answers to questions related to star formation at the extreme ends of the stellar initial mass function (IMF);

Scientific questions/goals of NIKA2

5 **Large Programs** on Guaranteed (*observational*) Time (1300h)
all of them linked to millimetre high angular resolution
and fast sky mapping of NIKA2

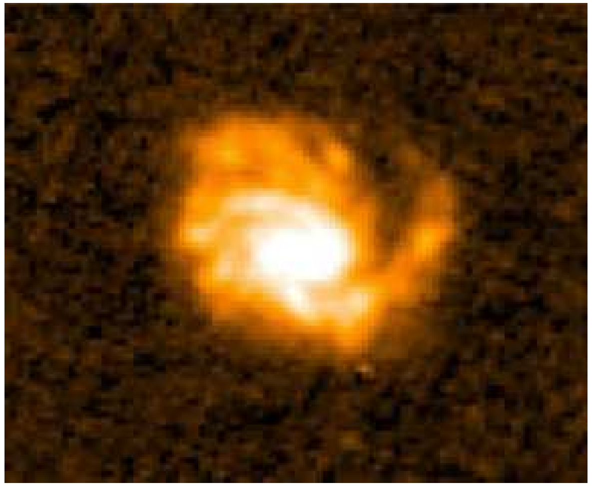

Nearby Galaxies

The mm part of the spectrum is one of the least explored parts of a galaxy's spectral energy distribution (SED), yet it contains emission from three fundamentally important physical processes: 1- thermal emission from dust, 2- free-free emission from ionized gas and 3- synchrotron emission from relativistic charged particles moving in the galactic magnetic field;

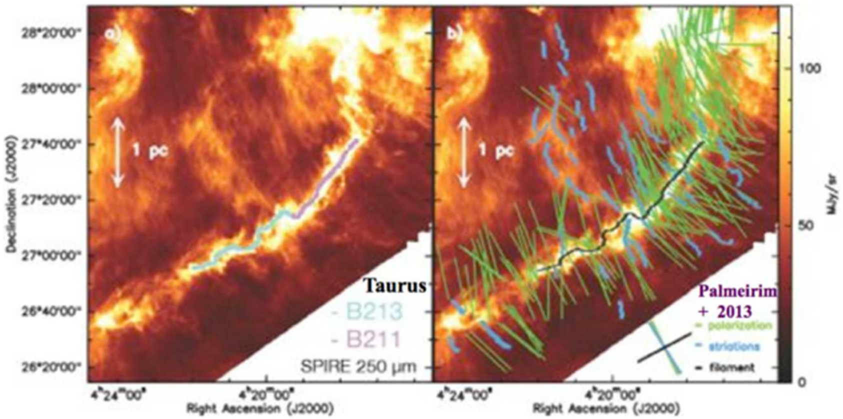

Polarization measurements of Galactic regions

1 mm polarization observations with NIKA2 camera would be to clarify the role played by magnetic fields in shaping the interconnected network of filaments and pre-stellar cores revealed by Herschel in Galactic molecular clouds.

5 **Large Programs** on Guaranteed (*observational*) Time (1300h)
all of them linked to millimetre high angular resolution
and fast sky mapping of NIKA2

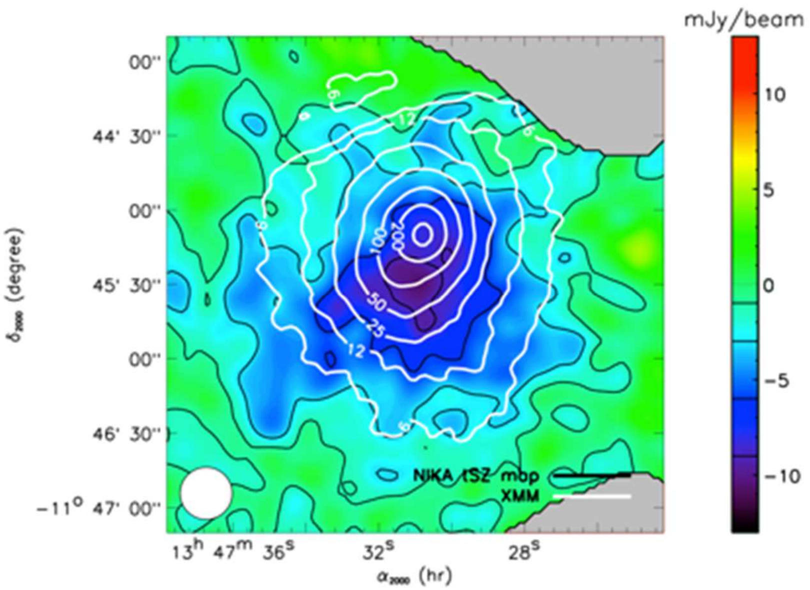

Clusters of galaxies
via the Sunyaev Zel'dovich effect

The LPSZ is finalized to observe a cosmologically representative, large sample of clusters (45) with redshift between 0.5 and 0.9 and mass range from 3 to 11 x $10^{14} M_{\odot}$.

The main output of the program is the study of the redshift evolution of the cluster ICM pressure profile as well as that of the scaling laws relating the cluster global properties, the Y (integrated Compton parameter) and T (temperature) for example, to their mass.

NIKA2 data are combined with ancillary data including X-rays and optical observations to significantly improve the use of clusters of galaxies to draw cosmological constraints.

Scientific questions/goals of NIKA2

Besides the LPs, several Observation Time proposals with specific targets have been completed or are in progress or may still be proposed.

Deadlines are around mid-March and mid-September of each year for the summer (01 June - 30 November) and winter (01 December - 31 May) scheduling periods.

https://oms.iram.fr/oms/

5 **Large Programs** on G *rvational*) Time (1300h)
all of them lin ular resolution
st sky mapping of NI 2

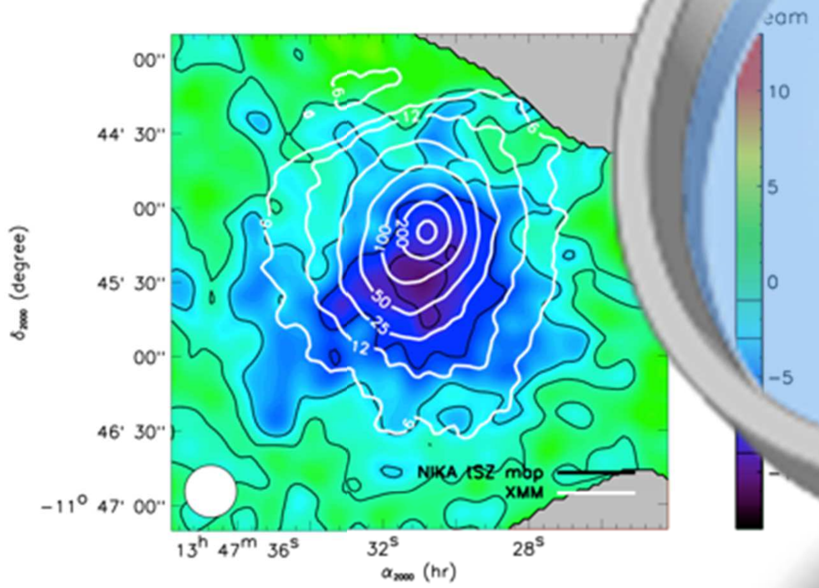

Clusters of galaxies
via the Sunyaev Zel'd n effect

The **LPSZ** is finalized serve a cosmologically representative, large e of clusters (45) with redshift between 0 0.9 and mass range from 3 to 11 x $10^{14}M_{\odot}$.

The main gram is the study of the ICM pressure profile as well as that of the s ating the cluster global properties, the Y ompton parameter) and T (tempe mple, to their mass.

NIKA2 data are combined with luding X-rays and optical observations nprove the use of clusters of galaxies to d gical constraints.

Clusters of galaxies = "Largest gravitationally bound structures in the Universe"

- Formed by gravitational collapse at the intersection of cosmic filaments in the Cosmic Web, correspond to massive Dark Matter halos
  - – Self-similar scenario: clusters are scaled copies of each other
  - – However, baryonic physics in the IntraCluster Medium (ICM) plays a significant role

- Total mass $10^{13} \div 10^{15}$ $M_{\odot}$, 10-1000 galaxies, T_e $10^7 \div 10^8$K, size ~Mpc, $0 < z < 3$
  composition: ~85% Dark Matter, ~13% gas (ICM), ~2% stars
- Mass and redshift distribution of clusters is sensitive to cosmological parameters

For these reasons, galaxy clusters form **ideal laboratories** for understanding

- o the underlying cosmology of our Universe

and

- o the physical processes driving galaxy evolution.

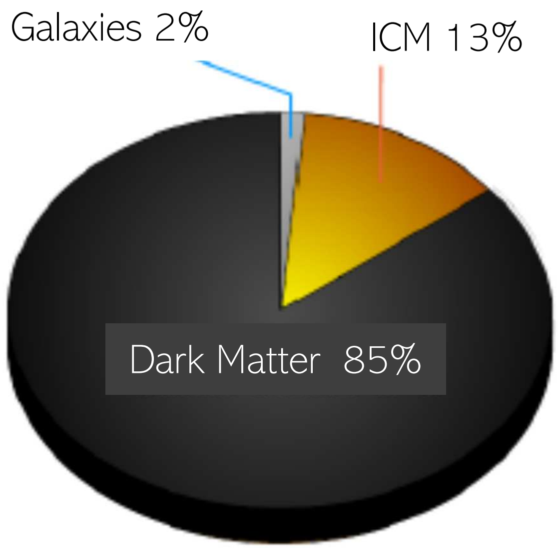

Clusters of galaxies = "Largest gravitationally bound structures in the Universe"

- Various cluster observables/components:

– Optical and infra-red emission: light from stars/galaxies
– X-ray emission: ICM e-
– Sunyaev-Zel'dovich effect (tSZ): Inverse Compton of CMB photons and hot ICM e-
– Radio halos: non-thermal emission from galaxies and ICM

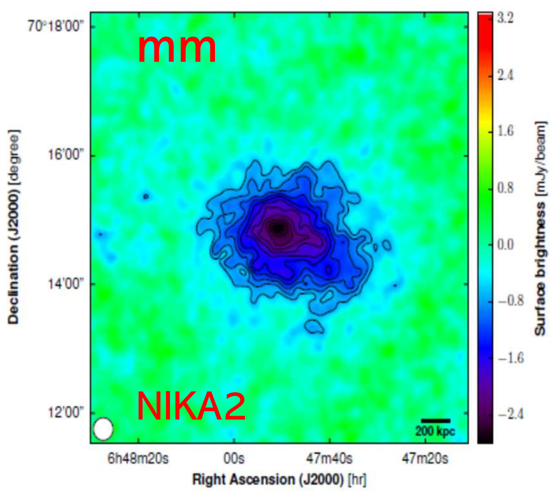

Compton parameter map

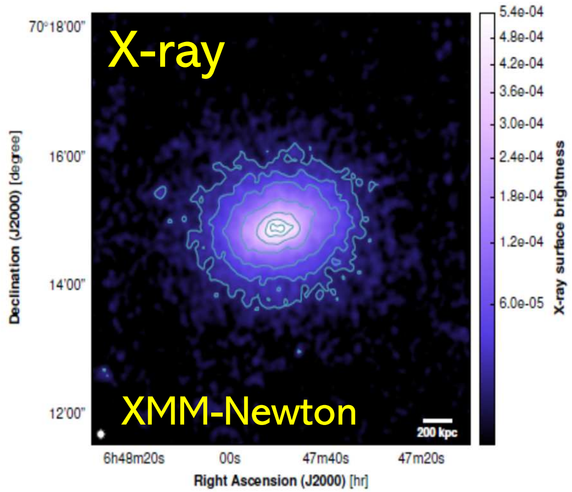

Photometry
Bremsstrahlung of the e-
Spectrometry
Line emission of the metal elements

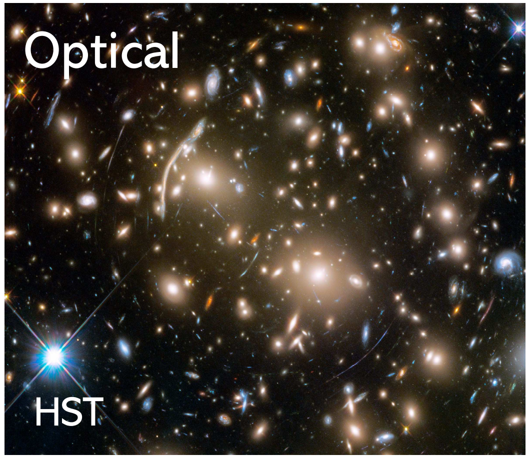

Strong and Weak lensing
Richness
Velocity dispersion

Sunayev-Zel'dovich Effect: basics

Thermal SZ component

CMB intensity distortion

$$\Delta I_\nu \approx I_0\, y \frac{x^4 e^x}{(e^x-1)^2}\left(x\frac{e^x+1}{e^x-1}-4\right) \equiv I_0\, y\, g(x)$$

$$x = h\nu/k_B T_{\rm CMB} \approx \nu/56.8\ {\rm GHz}; \qquad I_0 = \frac{2(k_B T_{\rm CMB})^3}{(hc)^2}$$

Compton parameter

$$y \equiv \int_{los} \frac{k_B T_e}{m_e c^2} d\tau_e = \int \frac{k_B T_e}{m_e c^2} n_e \sigma_T dl = \frac{\sigma_T}{m_e c^2}\int P_e\, dl$$

ICM pressure

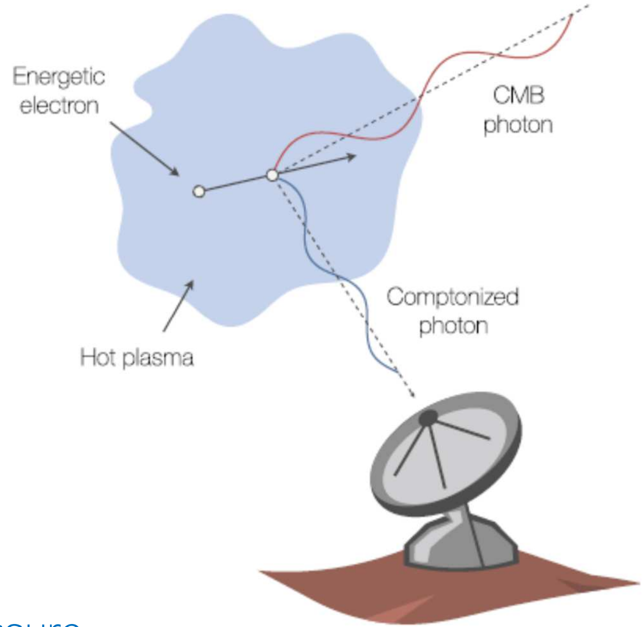

Kinematic SZ component

CMB intensity distortion

$$\Delta I_\nu \approx -I_0 \frac{x^4 e^x}{(e^x-1)^2} y_{\rm kSZ}$$

$$-y_{\rm kSZ} \equiv -\int_{los} \sigma_T n_e\, \boldsymbol{n}\cdot\boldsymbol{\beta}_p\, dl = -\int \boldsymbol{n}\cdot\boldsymbol{\beta}_p\, d\tau_e$$

cluster's peculiar motion

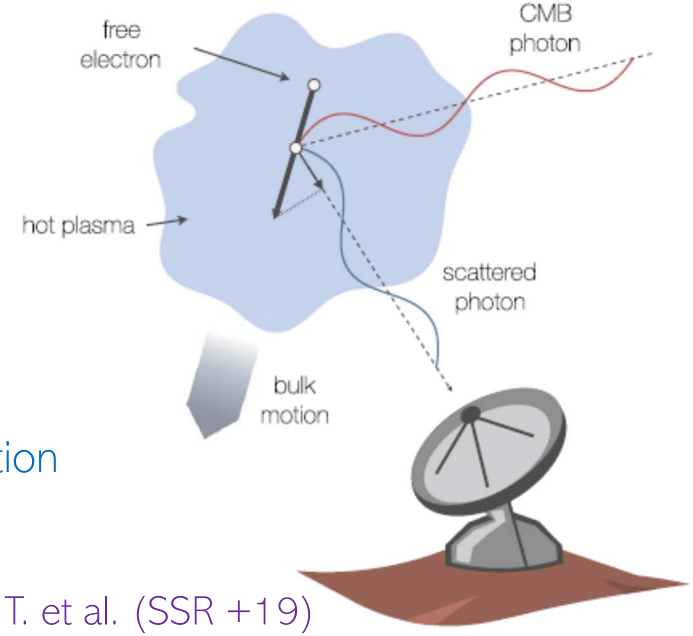

Zel'dovich Y.B., R.A. Sunyaev, Astrophys. Space Sci. (1969)
Sunyaev & Zel'dovich, Comm.A.S.P. (1972)

Mroczkowski T. et al. (SSR +19)

Focus on clusters of galaxies science by SZ effect

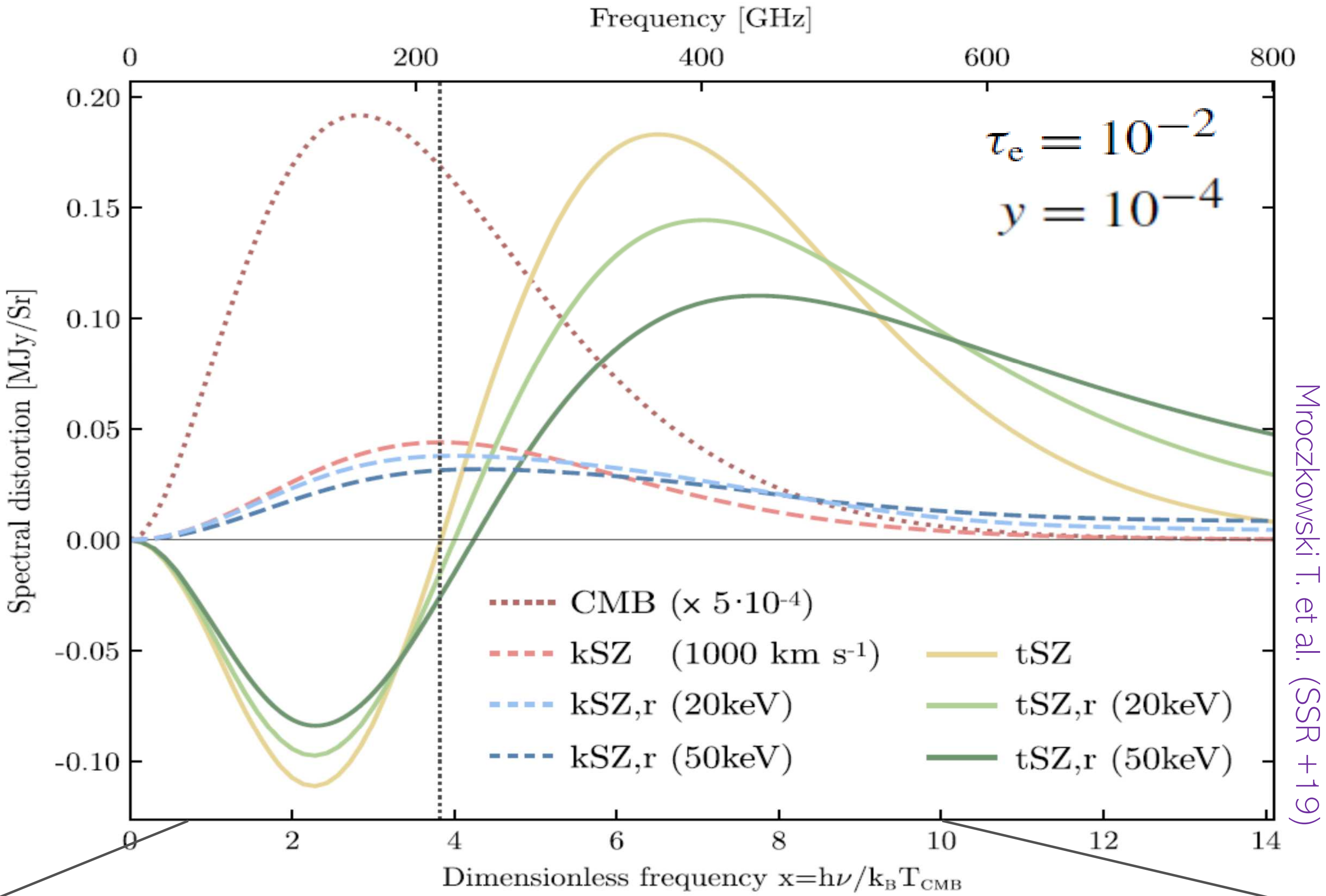

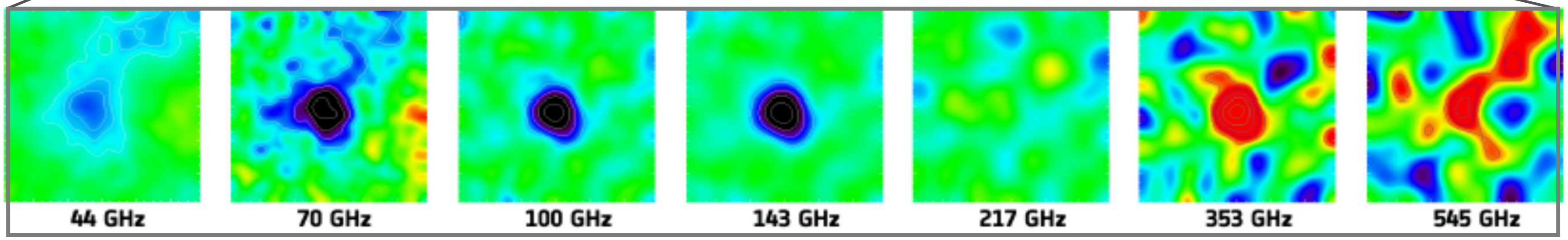

tSZ

Image credit: ESA / HFI & LFI Consortia

Clusters of galaxies = useful cosmological tools

we can infer
σ_8, the amplitude of the linear matter power spectrum at a scale of 8h^{-1}Mpc and
Ω_m, the total matter density of the universe
by
1- tSZ power spectrum amplitude

$$I_{\mathbb{P}} = \int x^2 \frac{\sin(\ell x/\ell_{500})}{\ell x/\ell_{500}} \mathbb{P}(x)\, dx$$

mean normalized gas pressure profile of the cluster population

$$C_\ell^{tSZ} = \int \frac{d^2V}{dzd\Omega} dz \int \frac{dn}{dM_{500}} \left| \frac{4\pi R_{500}}{\ell_{500}^2} \frac{\sigma_T}{m_e c^2} P_{500}\, I_{\mathbb{P}}(\ell_{500}) \right|^2 dM_{500}$$

2- Cluster number counts

$$\frac{d^2N}{dz\, dM_{500}} = \int \frac{d^2V}{dz\, d\Omega} \times \frac{dn}{dM_{500}} d\Omega$$

The mass (inside R_{500}) is not an observable!
It is inferred by applying different theoretical approaches (hydrostatic equilibrium, virial theorem, gravitational lensing, self-similarity assumptions, etc.)

Overdensity definition $\Delta = \frac{\rho_\Delta}{\rho_c(z)} = \frac{M_\Delta}{\frac{4}{3}\pi R_\Delta^3}$

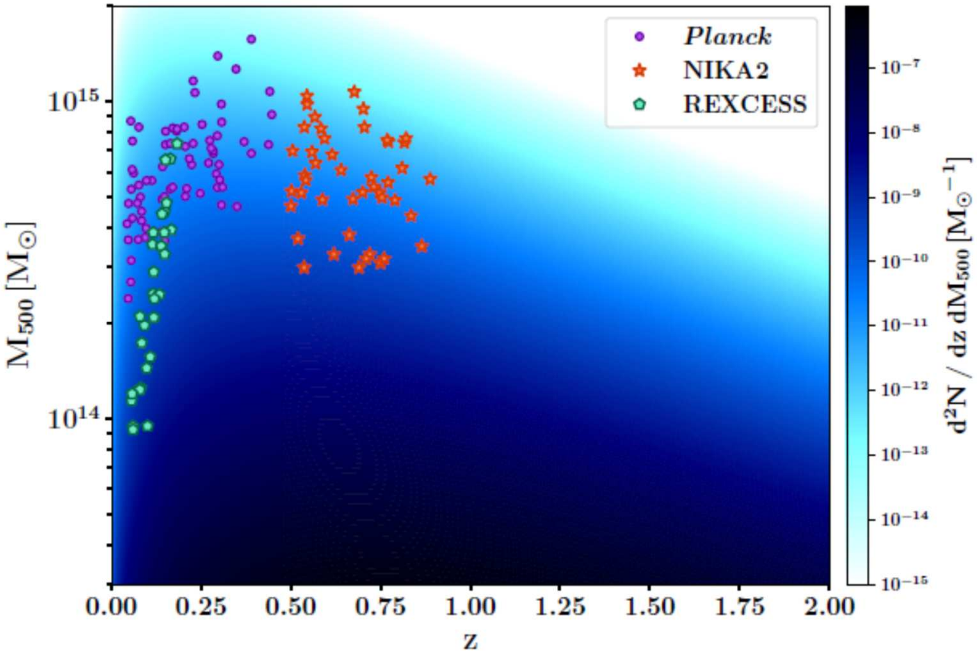

Ruppin F. et al. (MNRAS +19)

Clusters of galaxies = useful cosmological tools

but ….

a tension between cosmological constraints from CMB and Planck cluster catalogue exists and, even if reducing, is still to be investigated.

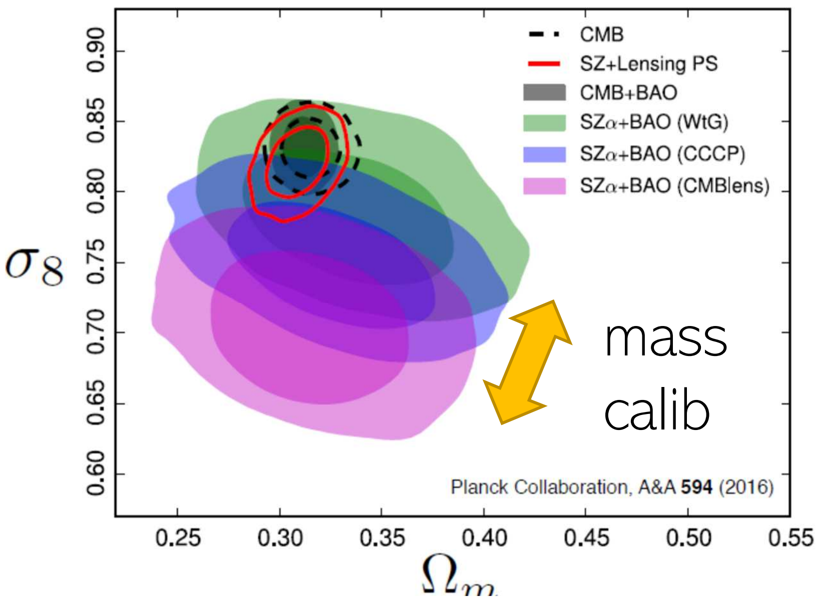

Planck collab XXIV, A&A (2016)

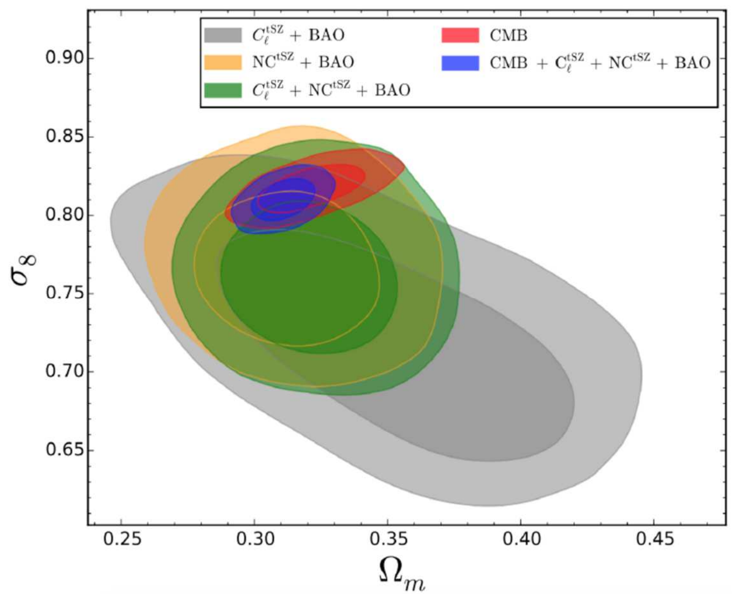

Salvati et al., A&A (2018)

clusters count constraints at 68% and 95% for the WtG, CCCP, and CMB lensing mass calibrations

tSZ power spectrum shows weaker constraints and clusters count still 1.5s inconsistent.

Clusters of galaxies = useful cosmological tools

but ….

a tension between cosmological constraints from CMB and Planck cluster catalogue exists and, even if reducing, is still to be investigated.

Possible suggestions to solve it

✓ Issues on ΛCDM model

(see neutrino mass, modified gravity et al.)

or

✓ Issues on Clusters of galaxies

1. Hydrostatic mass bias larger than expected
   but average mass bias around 10-20% Gianfagna G. MDP et al. MNRAS (2021)
2. Different ICM mean pressure profiles and scaling relations at high redshifts
   remember that Planck pressure profiles and Y-M scaling law calibrated in the low redshift range (z<0.5) Planck XX. A&A (2014)

Is the cluster total mass correctly estimated by hydrostatic equilibrium assumption?

No …. Mass Bias

$$\boxed{b = \frac{M_{\rm true} - M_{\rm HE}}{M_{\rm true}}}$$

$$M_{HE}(<r) = -\frac{r^2}{G\mu m_p n_e}\frac{dP_{therm}(r)}{dr}$$ SZ (+X)

$$M_{HE}(<r) = -\frac{rk_BT(r)}{G\mu m_p}\left[\frac{d\ln n_e(r)}{d\ln r} + \frac{d\ln T(r)}{d\ln r}\right]$$ X (+SZ?)

Gianfagna, MDP, et al. (2021)

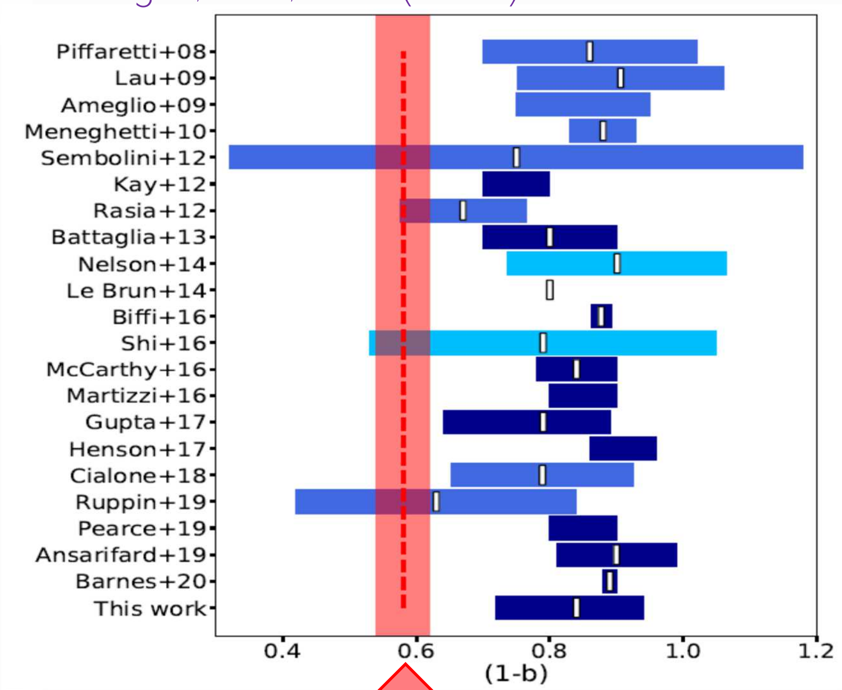

Radial profiles of gas density, pressure and temperature

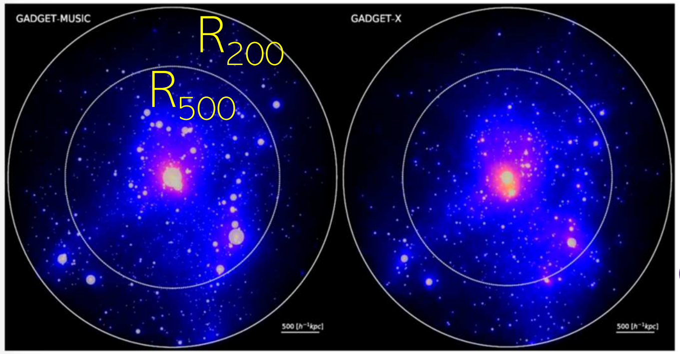

The Three Hundred
Hydrodynamical simulations
Cui W., MDP, et al. MNRAS (2018)

- bias$_{SZ}$ and bias$_X$ at 0<z<1
- Correction with non-thermal pressure components or ICM clumpiness
  Ansarifard, MDP, et al. MNRAS (2020)
- Mild correlation with cluster dynamical state
  Cialone G., MDP, et al. MNRAS (2018); De Luca, MDP et al. (2021); Capalbo V., MDP et al. (2021)

by the way, $b = 0.4$ would solve the tension with CMB data Salvati et al. A&A (2019)

Focus on clusters of galaxies science by SZ effect

The knowledge of ICM pressure profiles is mandatory, but also for distant clusters…

The widely used mean cluster ICM pressure profile is the **gNFW model** Nagai D. et al. ApJ (2007)

$$\frac{P(r)}{P_{500}} = \frac{P_0}{x^c(1+x^a)^{\frac{b-c}{a}}}$$

$$x = r/r_s \qquad r_s = R_{500}/c_{500}$$

$$P_{500} = 1.65 \times 10^{-3} E_z^{8/3} \left[\frac{M_{500}}{3 \times 10^{14} h_{70}^{-1} M_{\odot}} \right]^{2/3} h_{70}^2 keV/cm^3$$

Parameters have been tuned on massive and low redshift clusters (z<0.4)

- Arnaud et al. (2010) from REXCESS catalogue (X) + 3 hydrosims
- Planck collab. (2013) from 62 clusters (SZ)

already slight differences on the outer slopes

Pressure profiles for synthetic clusters: local, distant and with different dynamical state

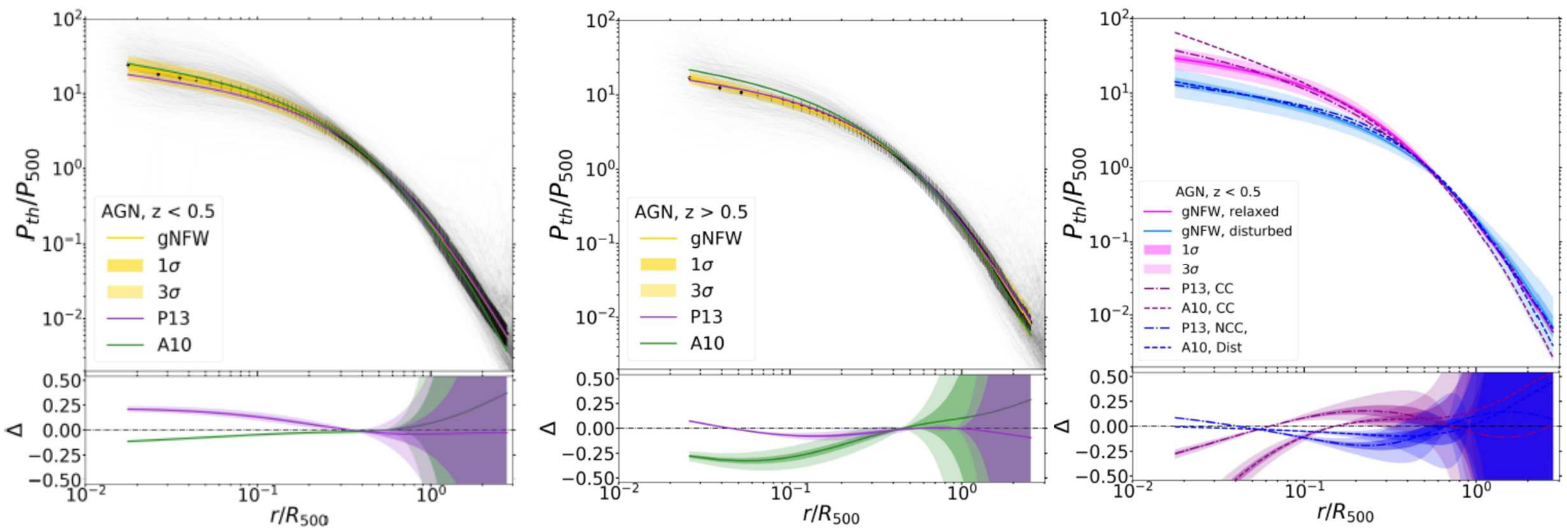

MUSIC Hydrodyn simulations

Gianfagna, MDP, et al. MNRAS (2021)

Scaling Laws: self-similar relation between mass and observables

The temperature, entropy and pressure profiles are normalized to the values computed for the given cluster mass using a simple self-similar model Kaiser N. MNRAS (1986); Voit G.M Rev MP (2005)
Many other observables are also related to cluster total mass, e.g. integrated Compton parameter.

$$E^{-2/3}(z)\left[\frac{D_A^2\, Y_{500}}{10^{-4}\,\mathrm{Mpc}^2}\right] = 10^{-0.19\pm0.02}\left[\frac{(1-b)M_{500}}{6\times10^{14}\,M_\odot}\right]^{1.79\pm0.08}$$

Planck calibrated Y-M scaling law

observable

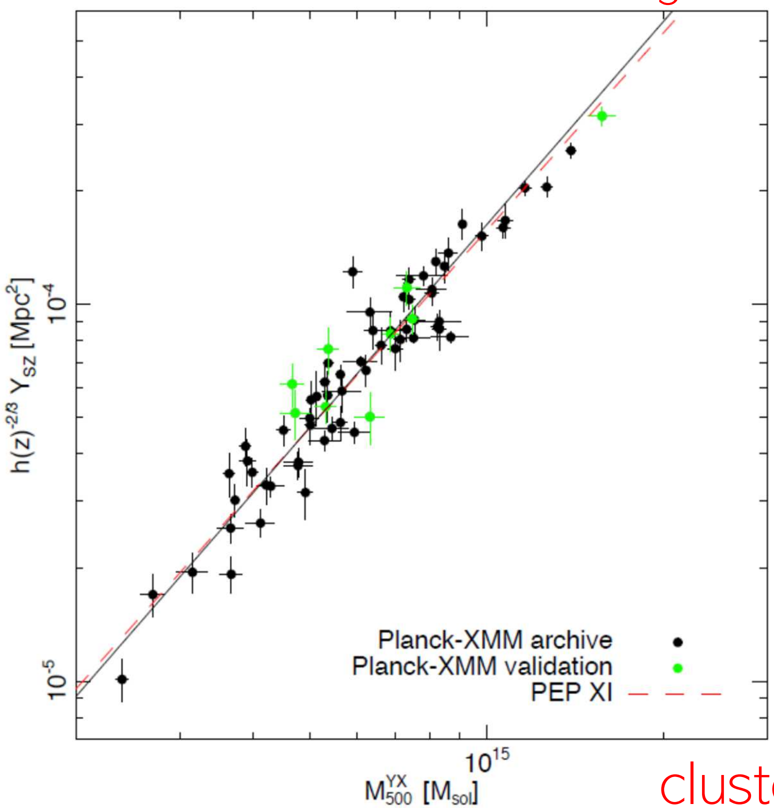

cluster total mass

Comparison with Hydro-simulations

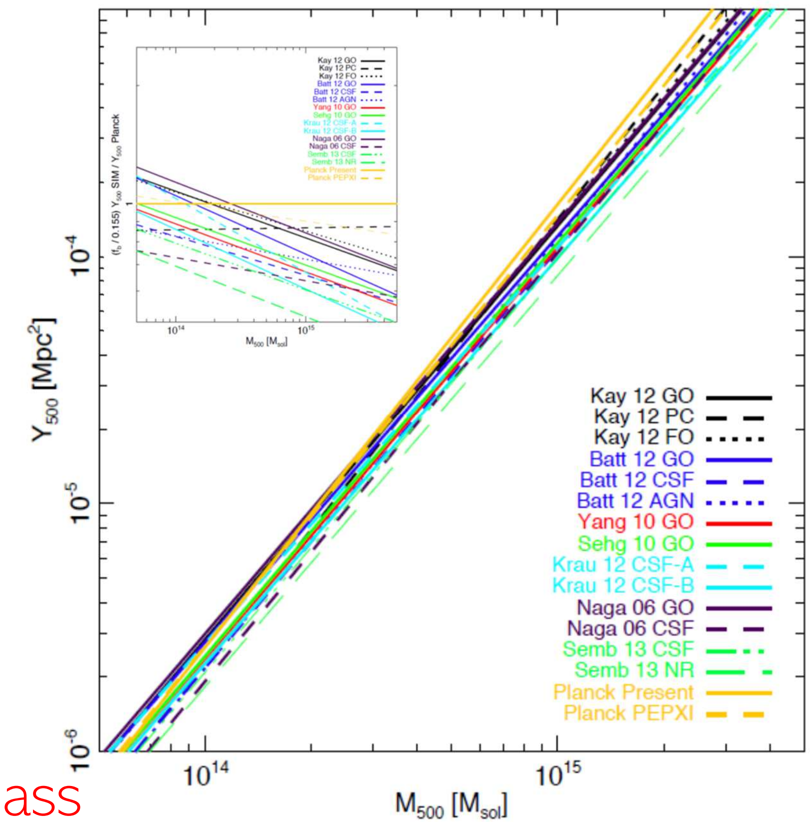

Planck collab XX, A&A (2014)

Need of a more robust calibration of the mass-observable as function of:

- **redshift**
- **cluster internal matter distribution**

High angular resolution observations of high redshift clusters are required for accurate cosmology with clusters investigating in detail

Y-M relation, mean pressure profile and mass inference

This is the goal of NIKA2 LPSZ !

The key ingredients for high sensitive/resolution mm-SZ observations

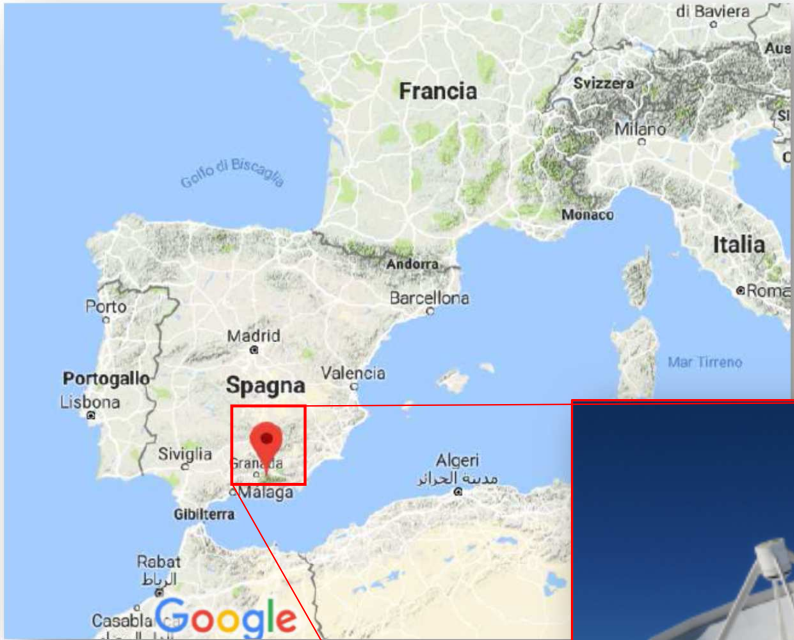

Site

Pico Veleta 2800 m a.s.l. (Spain)

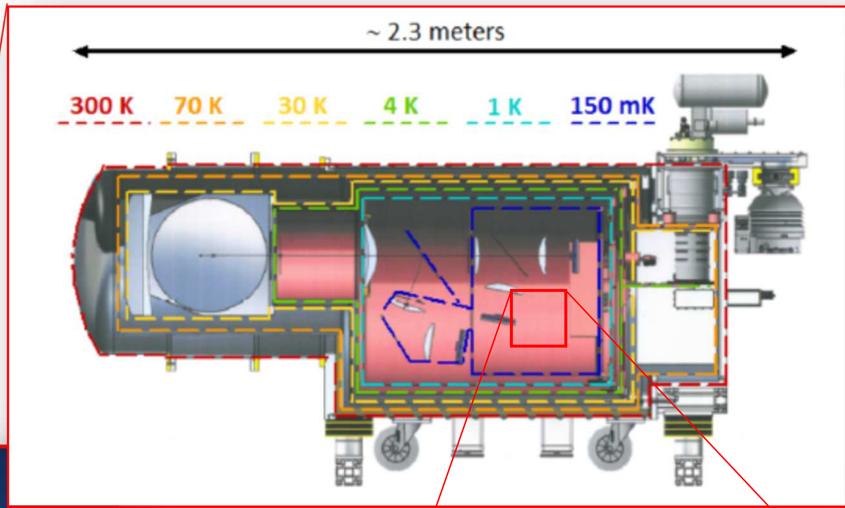

Cryostat

1.3 tons to cool down to 150mK

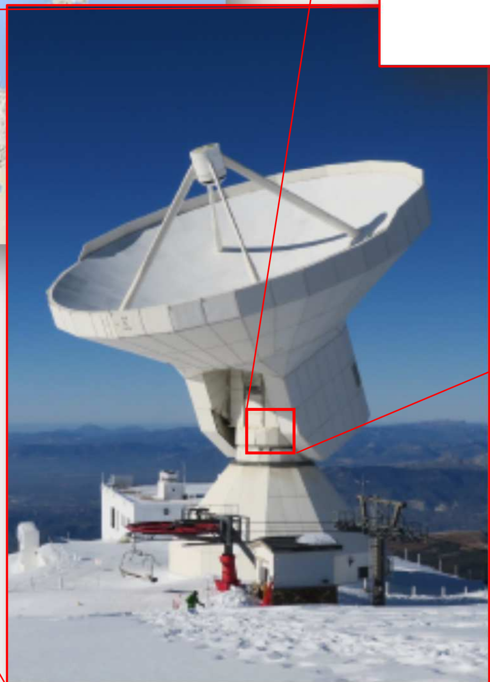

Telescope

30m IRAM single dish

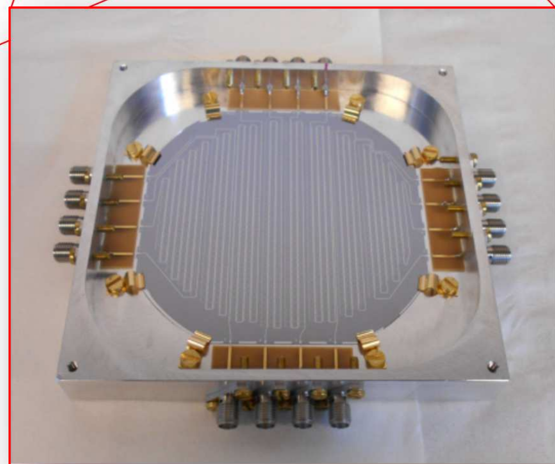

Detectors

3 k-pixels KID cameras

The observational impacts: **Site**, *i.e. good opacity conditions @ mm-waves*

Table 1. Characteristics of the Pico Veleta site

Location	
Pico Veleta, Sierra Nevada, 45 km from Granada, Spain	
Telescope coordinates	
Altitude	2870 m (elevation axis)
Geographical longitude	03°23′58″.1 West
Geographical latitude	37°04′05″.6 North
Climate	
Number of days and nights with >75% clear sky	200 per year
Average wind velocity	8 m s^{-1}
Maximum wind velocity	50 m s^{-1}
Maximum summer temperature	20 °C
Minimum winter temperature	−15 °C
Average diurnal variation	5 °C
Precipitable water vapor to zenith	
Average summer	4 mm
Average winter	2 mm
Typical good zenith transmission at 1.2 mm wavelength	0.90

Baars J.W.M. et al. (A&A 1987)

https://www.iram-institute.org/

The observational impacts: **Site**, *i.e. good opacity conditions @ mm-waves*

Table 1. Characteristics of the Pico Veleta site

Location	
Pico Veleta, Sierra Nevada, 45 km from Granada, Spain	
Telescope coordinates	
Altitude	2870 m (elevation axis)
Geographical longitude	03°23′58.″1 West
Geographical latitude	37°04′05.″6 North
Climate	
Number of days and nights with >75% clear sky	200 per year
Average wind velocity	$8\,\mathrm{m\,s^{-1}}$
Maximum wind velocity	$50\,\mathrm{m\,s^{-1}}$
Maximum summer temperature	20 °C
Minimum winter temperature	−15 °C
Average diurnal variation	5 °C
Precipitable water vapor to zenith	
Average summer	4 mm
Average winter	2 mm
Typical good zenith transmission at 1.2 mm wavelength	0.90

Baars J.W.M. et al. (A&A 1987)

Why?

https://www.iram-institute.org/

The observational impacts: **Site**, *i.e. good opacity conditions @ mm-waves*

optical depth
i-th air component

$$\tau_i(\lambda, z_0) = \int_{z_0}^{\infty} r_i(z)\rho(z)\kappa_i(\lambda)dz$$

mass extinction coefficient

dry air density

site altitude

mixing ratio

intensity attenuation

$$I(z_0) = I_0 exp\left[-\frac{1}{\cos\theta}\sum_i \tau_i(\lambda, z_0)\right]$$

secant-law

zenith angle

The net result for having low opacity conditions is **low pwv**
i.e. the main air component to affect mm-waves attenuation

The observational impacts: **Site**, *i.e. good opacity conditions @ mm-waves*

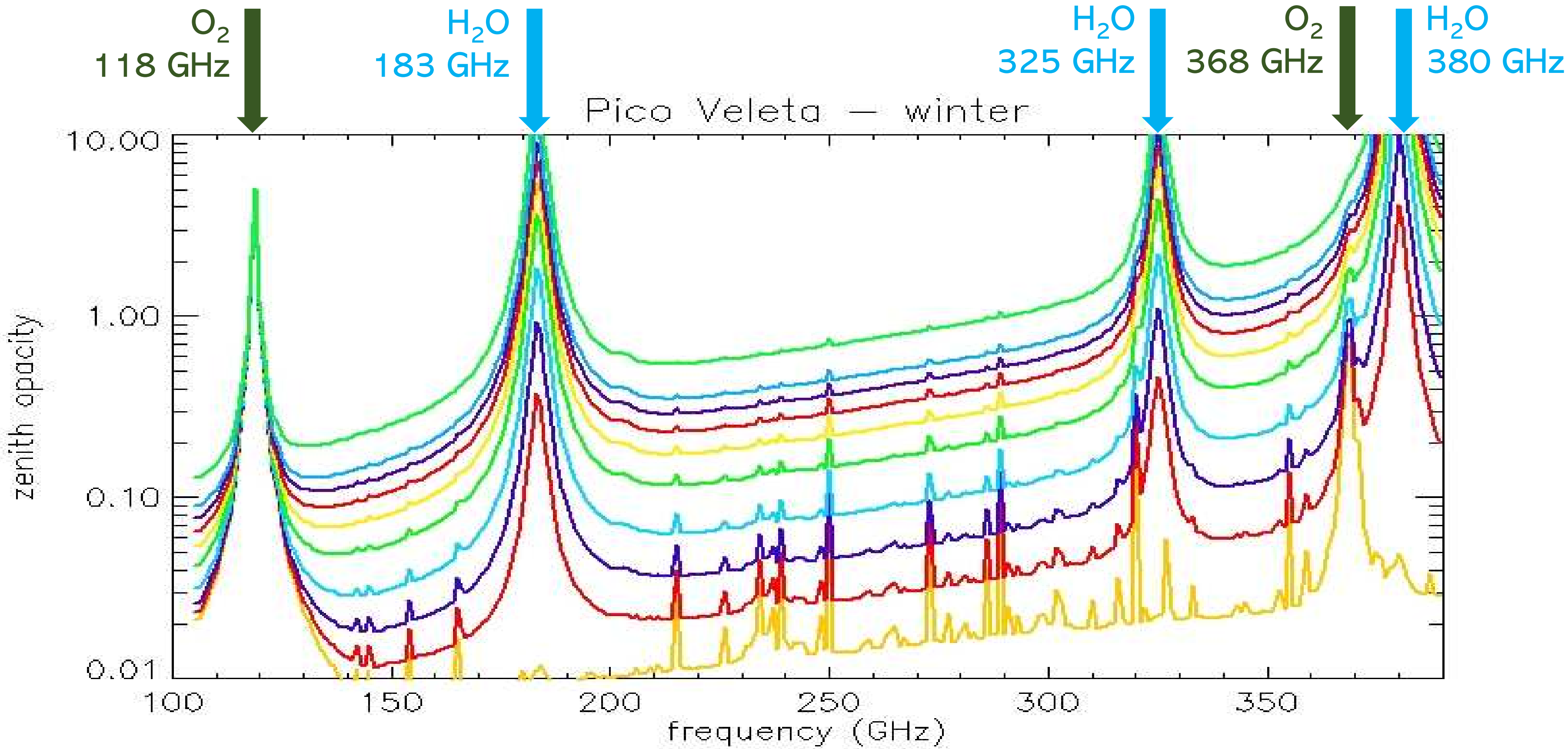

ATM model

Atmospheric Transmission at Microwaves Opacity 100 GHz – 2 THz

ATM zenith opacity: 0.1 < pwv(mm) < 6.0

Pardo J.R., et al. (IEEE +01)

The observational impacts: **Site**, *i.e. good opacity conditions @ mm-waves*

IRAM taumeter measurements

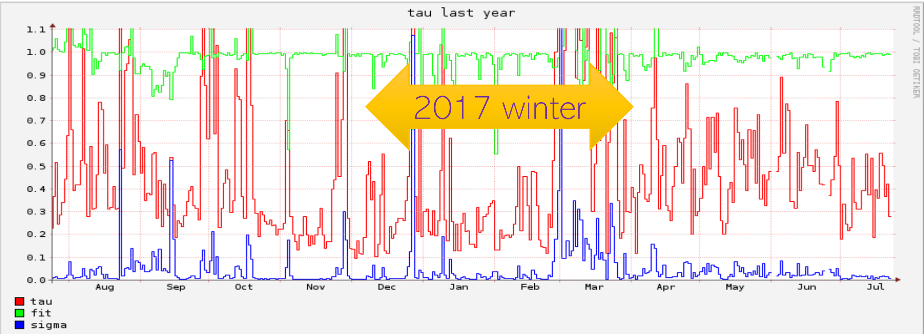

zenith opacity at 225 GHz

Good in-bands opacity conditions

$\tau < 0.2$ + stability

(but it depends on the different targets)

Adam R., MDP et al. (A&A +18)

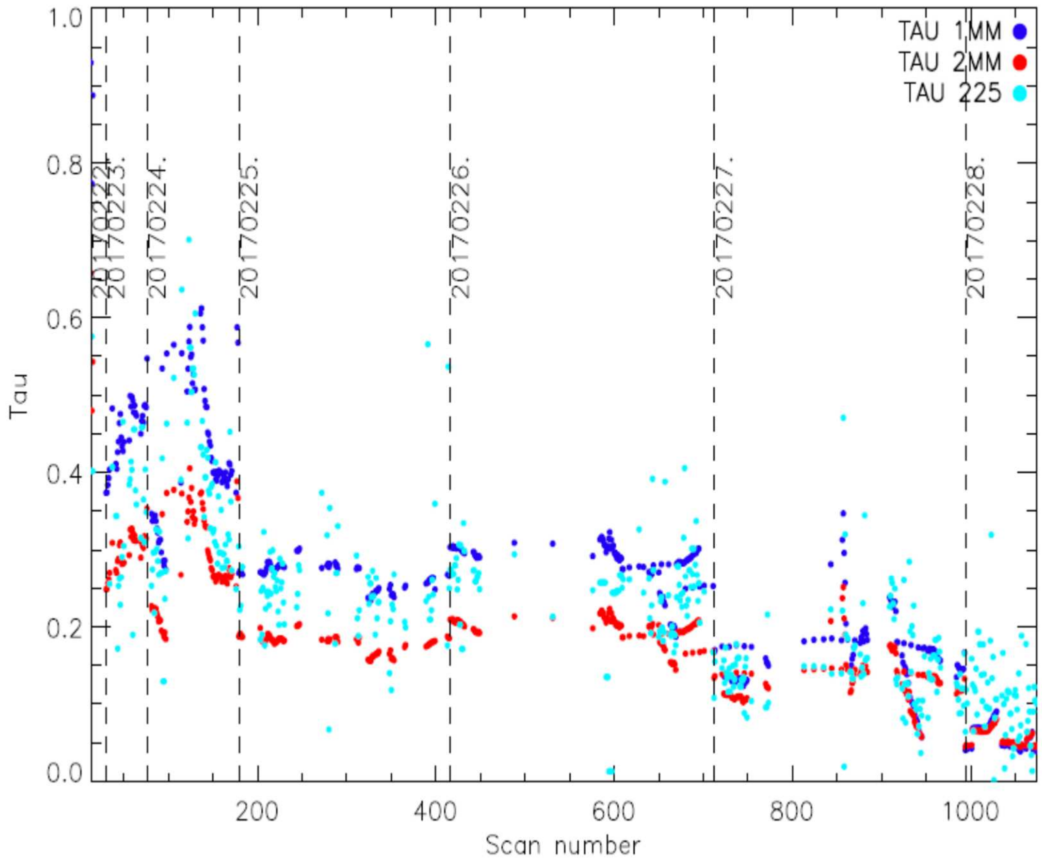

NIKA2 commissioning campaign

February 2017

Site Photometric Quality Ratio

$$\mathrm{SPQR} = \frac{\langle T \rangle}{\sigma_T}$$

Averaged transmission

Transmission fluctuations

De Gregori S. MDP et al. (MNRAS +12)

The observational impacts: **Telescope**, *i.e. high angular resolution*

30m IRAM telescope (MRT)
Cassegrain Configuration

Paraboloidal main reflector:	
diameter	$D = 30\,\mathrm{m}$
focal length	$f = 10.5\,\mathrm{m}$
focal ratio	$f/D = 0.35$
Hyperboloidal subreflector:	
diameter	$d = 2.0\,\mathrm{m}$
eccentricity	$e = 1.0746$
Nasmyth reflectors (flat):	
size	$d_n = 1.0 \times 0.7\,\mathrm{m}$
Cassegrain magnification factor:	$M = 27.8$
Effective focal ratio of Nasmyth:	$f_e/D = 9.73$
Distance from prime to secondary focus:	$f_c = 19.79\,\mathrm{m}$

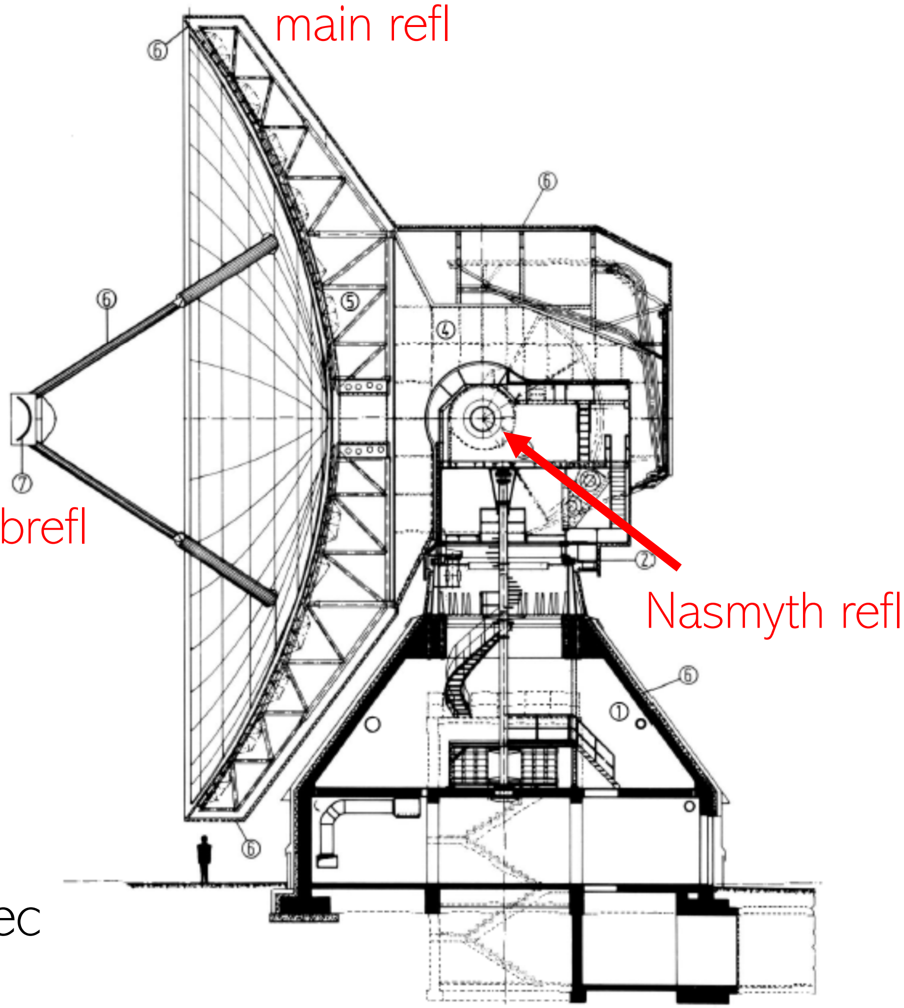

Alt-az mount with pointing accuracy ~1÷3 arcsec
... in operation since 1985

Baars J.W.M. et al. (A&A 1987)

The observational impacts: **Telescope**, *i.e. high angular resolution*

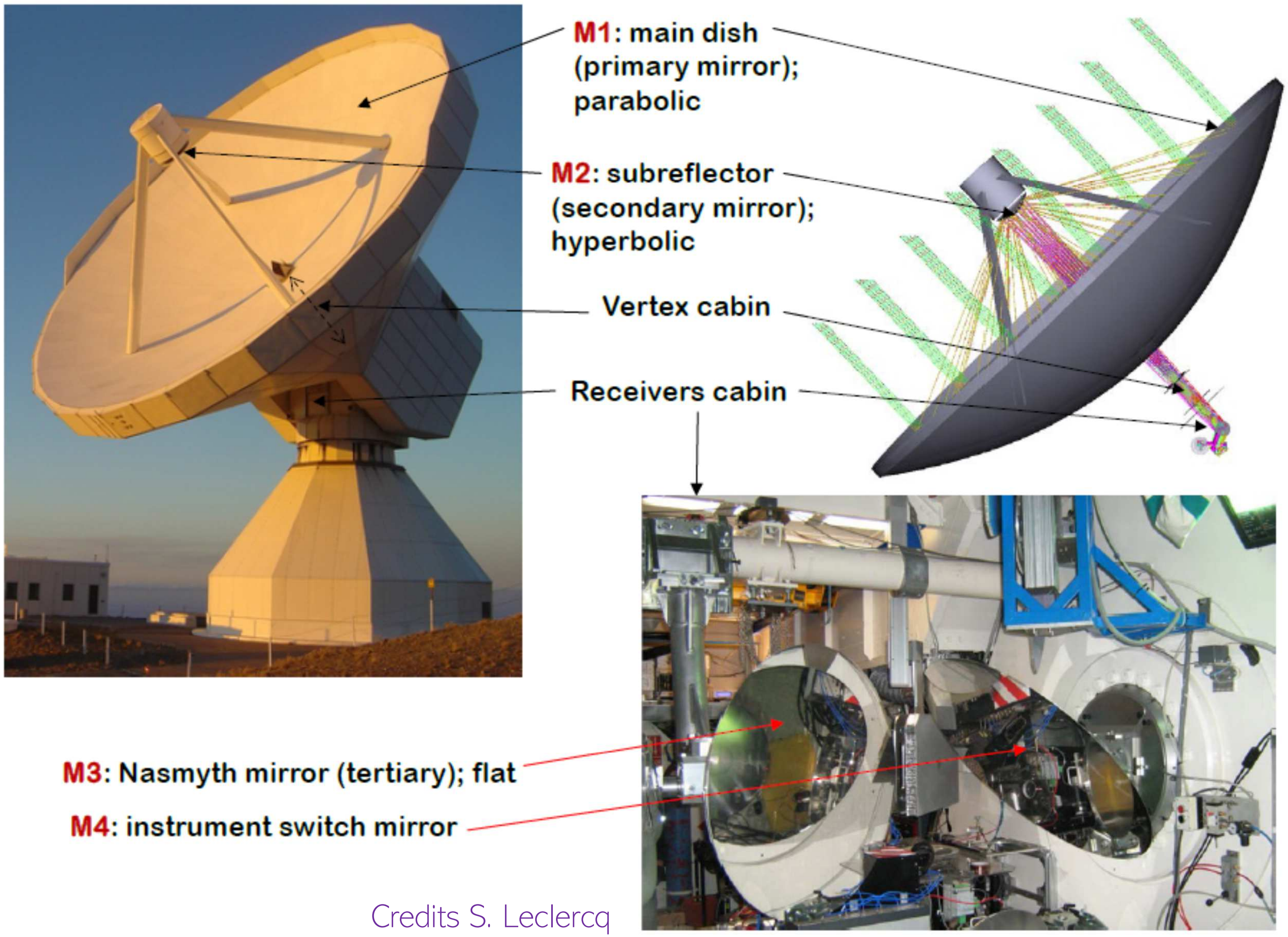

Credits S. Leclercq

The observational impacts: **Telescope**, *i.e. high angular resolution*

Large single dish **(M1-M2)** plus warm optics **(M3-M6)** plus cold relay optics **(M7-M8)**

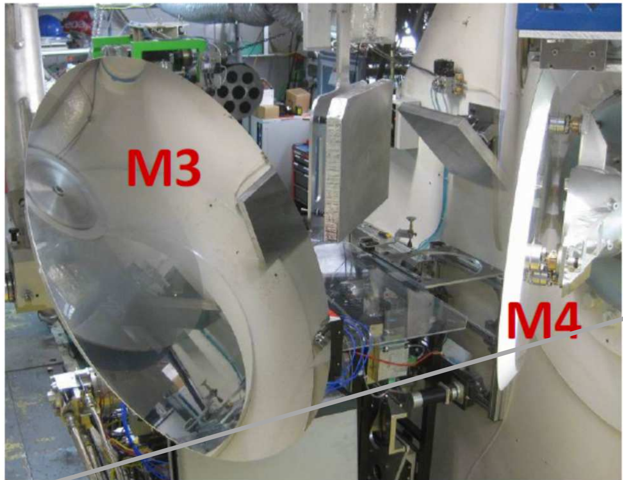

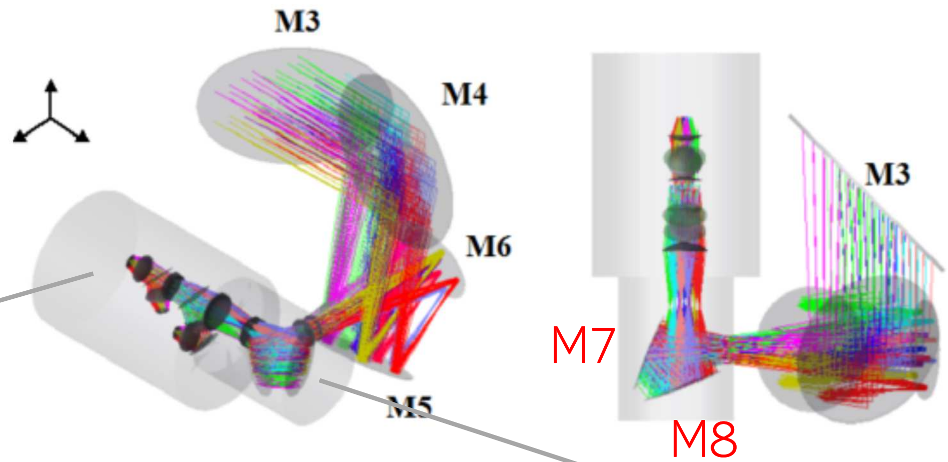

DLFoV
6.5 arcmin

mapping speed

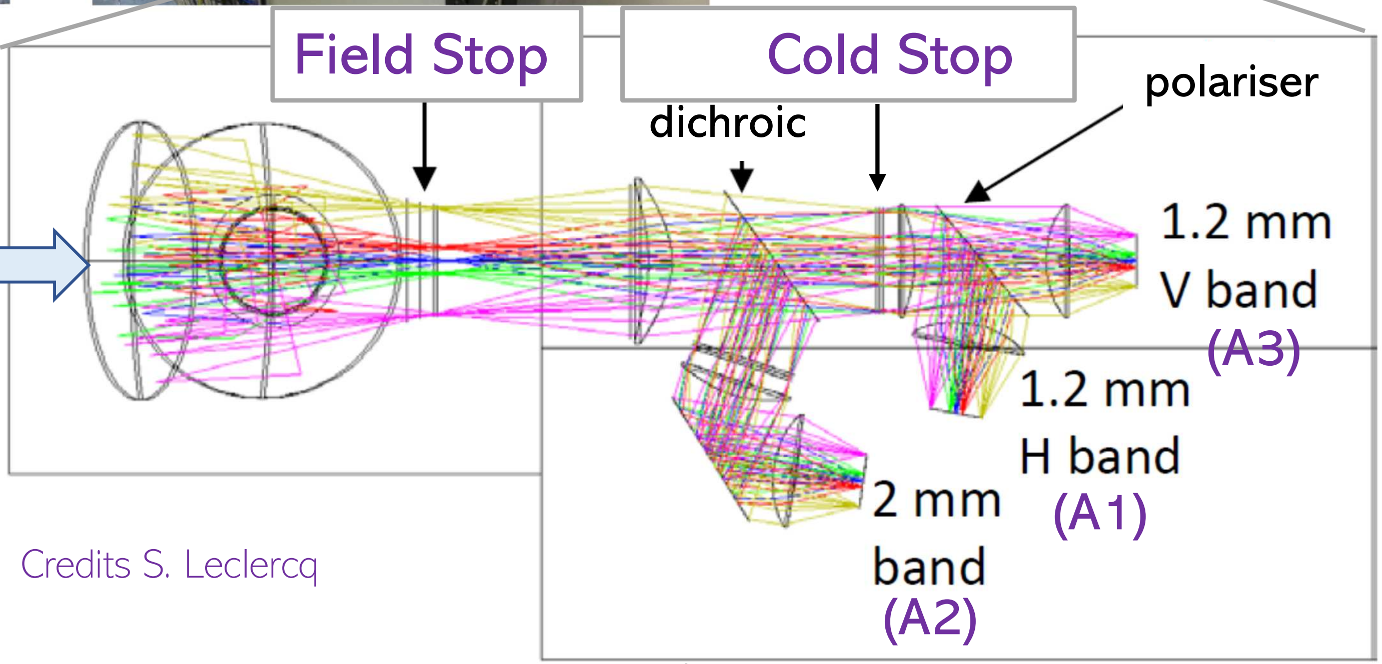

EP dia
27.5 m

angular resolution

Credits S. Leclercq

The observational impacts: **Telescope**, *i.e. high angular resolution*

Beam Pattern Maps (dB)

quadrupod secondary support structure

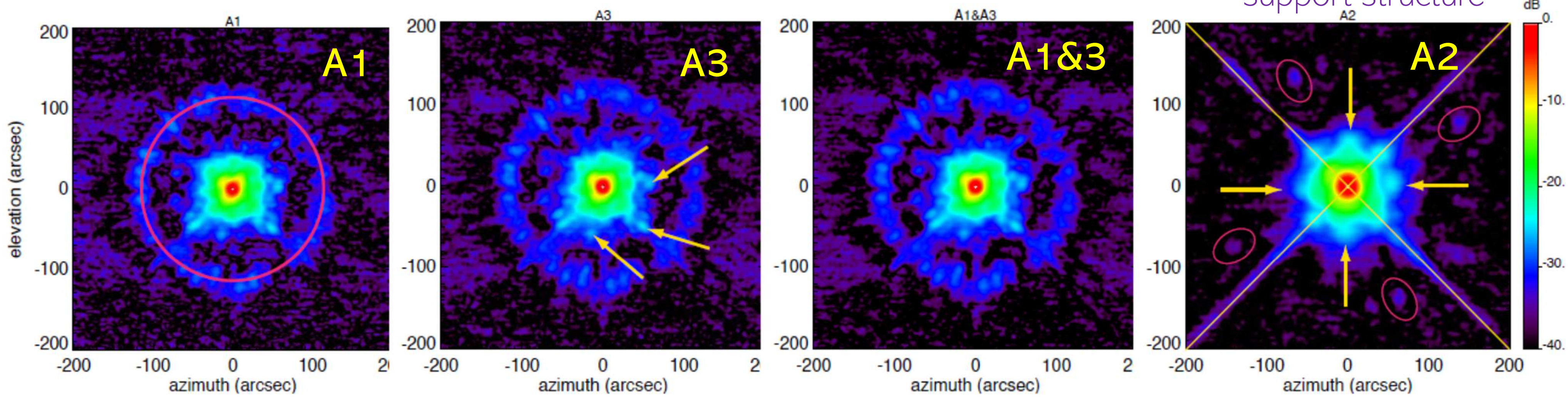

Perotto L., MDP et al. (A&A +20)

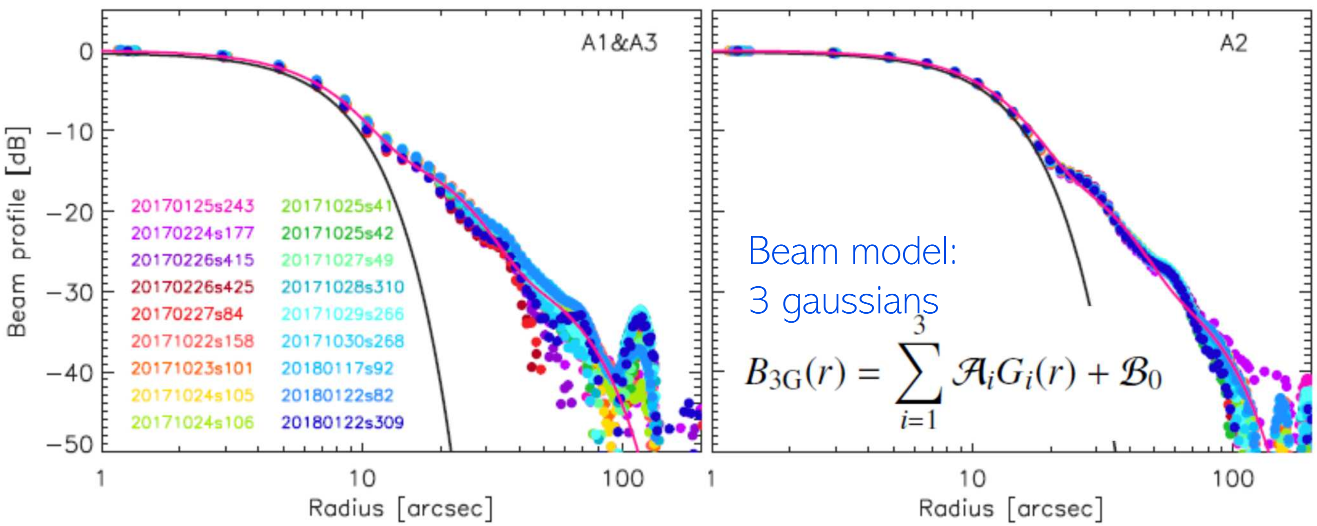

Main beams
(2D Gaussian FWHM avgs)

11.2" at 260 GHz (BE = 55%)
17.7" at 150 GHz (BE = 75%)

$$BE = \frac{\Omega_{mb}}{\Omega_{tot}} \qquad \Omega_{mb} = 2\pi\,\sigma_{mb}^2$$

$$FWHM = 2\sqrt{2\ln 2}\,\sigma_{mb}$$

The observational impacts: **Cryostat**, *i.e. cold optics and cold fingers*

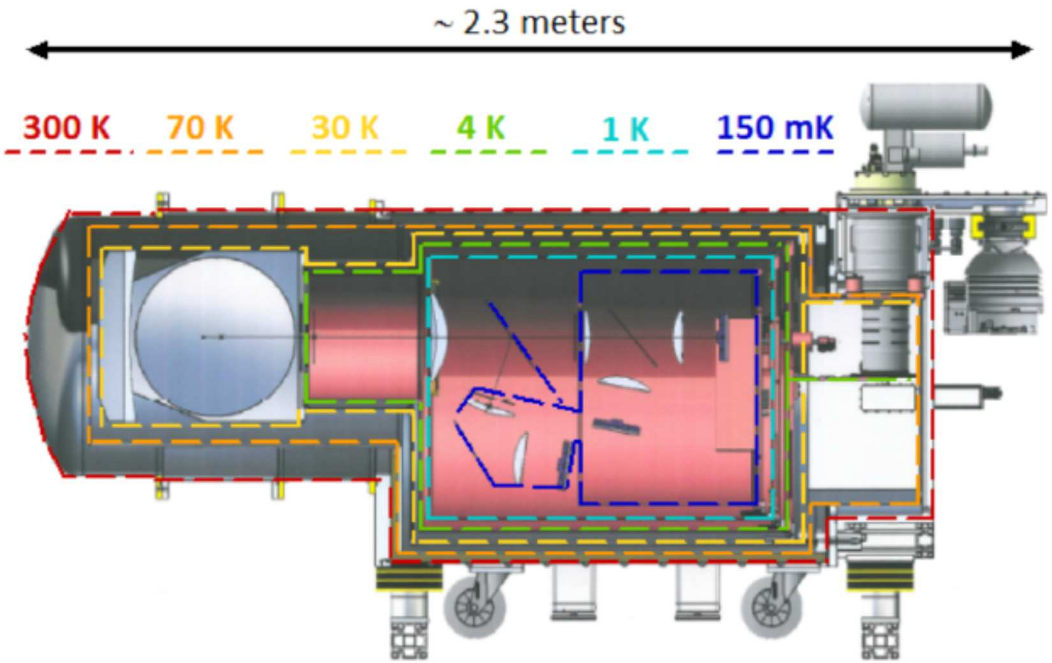

Usual Matryoshka-like cryo-approach

- ✓ 2 Pulse Tube cryocoolers (Cryomech PT415) working in parallel ⇒ 70-30K & 4 K
- ✓ 1 closed-cycle ^{3}He-^{4}He dilution fridge ⇒ **150 mK**
- ✓ The cool down process lasts 5 days
- ✓ Completely remote controlled without cryogens

The observational impacts: **Cryostat**, *i.e. cold optics and cold fingers*

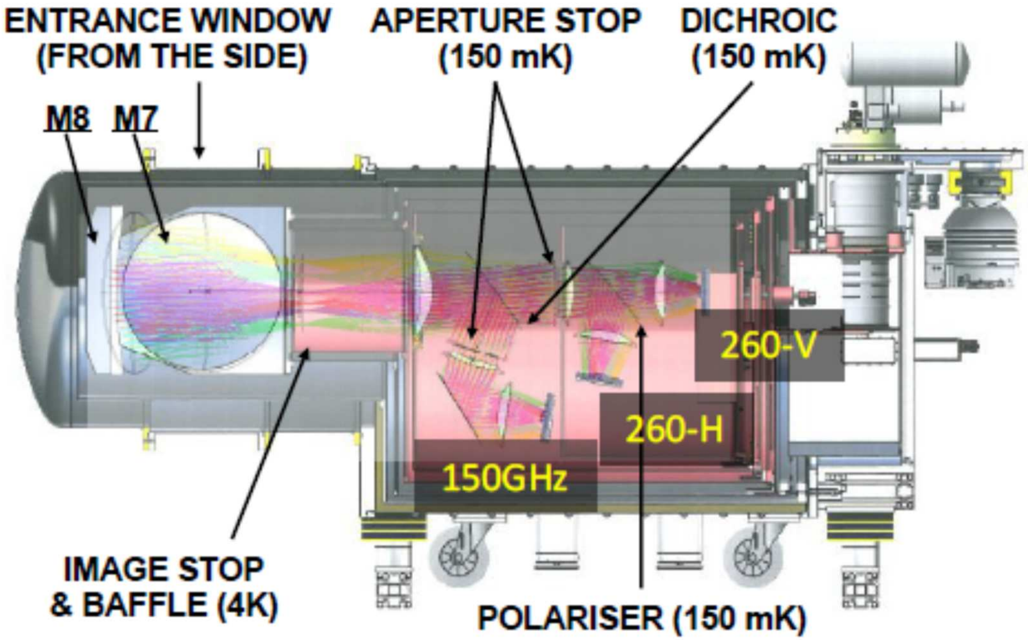

The **optical filtering chain** is composed by

- ✓ half-wave polarization modulator (only for polar-obs);
- ✓ multi-mesh filters (as thermal blockers);
- ✓ air-gap dichroic plate and
- ✓ grid polariser,

all at different thermal stages.

Goal: to limit and to select the spectral range and the radiative loading on the detectors

The observational impacts: **Cryostat**, *i.e. cold optics and cold fingers*

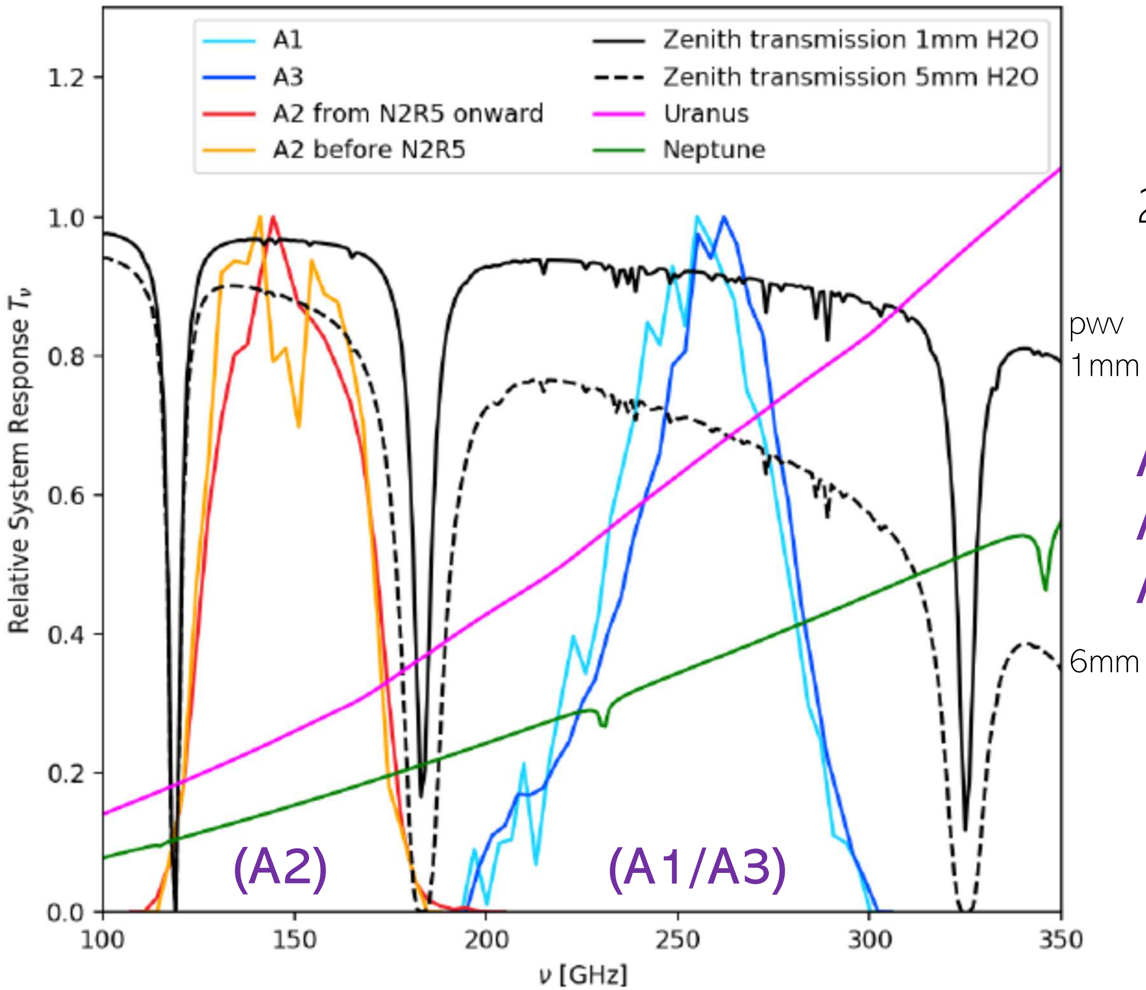

Perotto L., MDP et al. (A&A +20)

2 bands for 3 arrays (A1, A2 and A3)

A1: 260 GHz (BW=50 GHz) (H pol)
A2: 150 GHz (BW=40 GHz)
A3: 260 GHz (BW=50 GHz) (V pol)

The observational impacts: **Detectors**, *i.e. high sensitivity sensors*

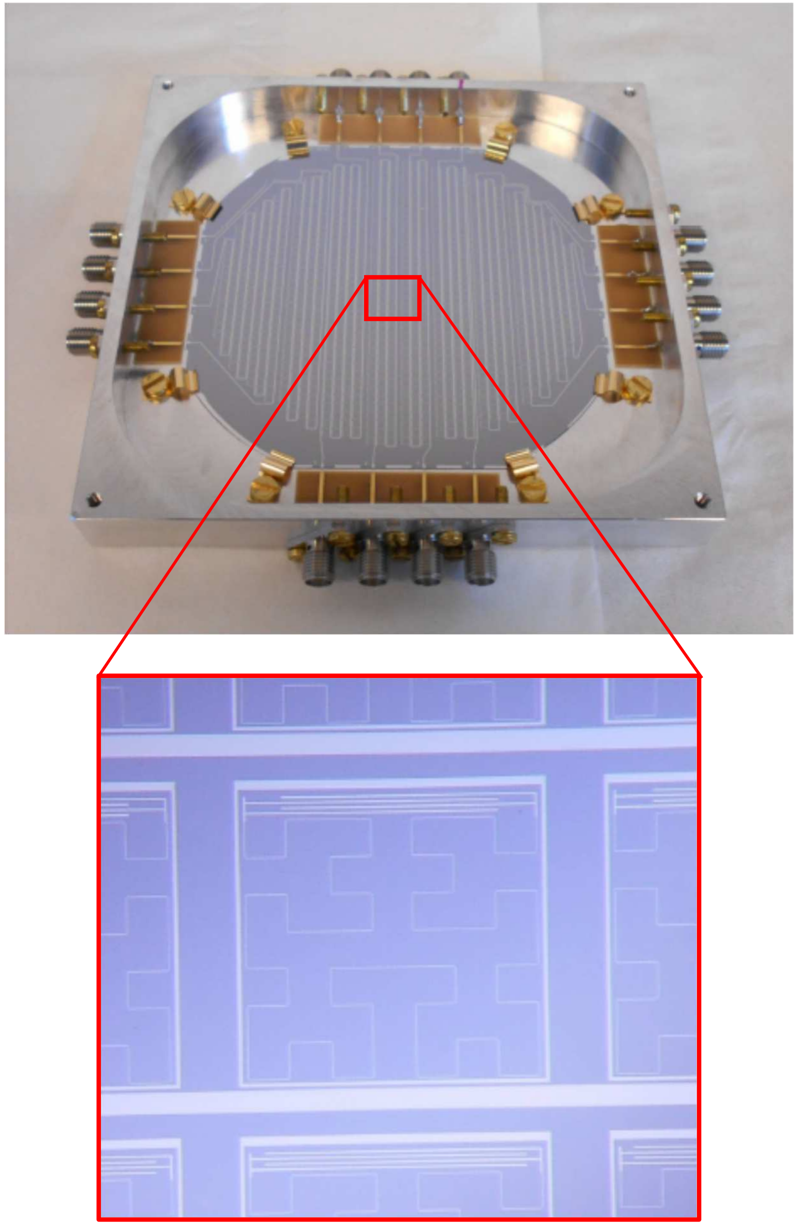

Kinetic Inductance Detectors

Cooper pairs broken by photons change kinetic inductance into a superconducting strip.

Aluminium superconducting resonators:
4" high-resistivity silicon wafers with e-beam deposited aluminium film Calvo M. et al. (JLTP+16)

Variation of resonance frequency dependent on inductance and therefore incoming radiation power

$$\boxed{\delta f_0 \propto \delta L_k \propto P_{opt}}$$

Array 150 GHz (A2) – 76 mm in dia.
616 pixels - size (Fλ) 2.8x2.8 mm^2
Arrays 260 GHz (A1 & A3)
1140 pixels - size (Fλ) 2x2 mm^2

Hilbert-shape absorbers/inductors Roesch et al. (+12)

The observational impacts: **Detectors**, *i.e. high sensitivity sensors*

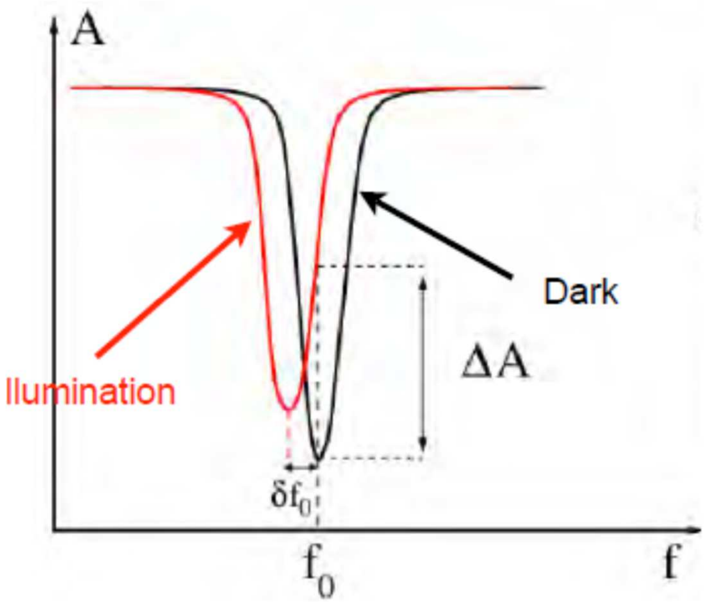

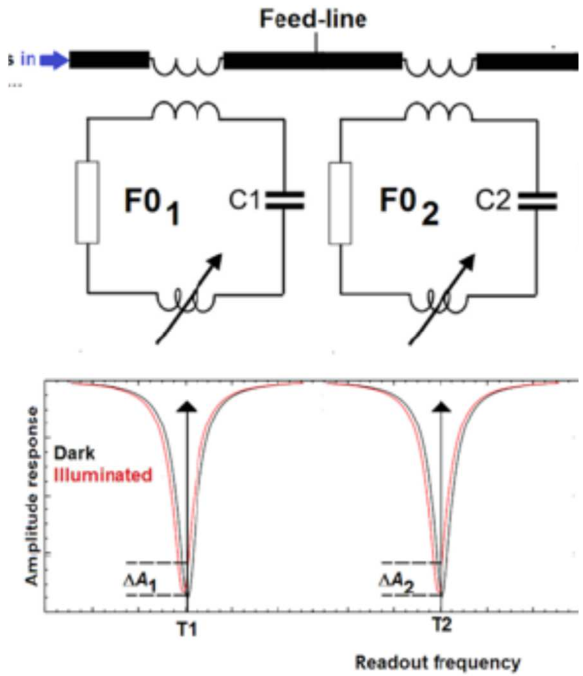

Natural frequency multiplexing capabilities making ideal approach for large matrix detectors

Limited number of coaxial cables from room to low temperature stages.

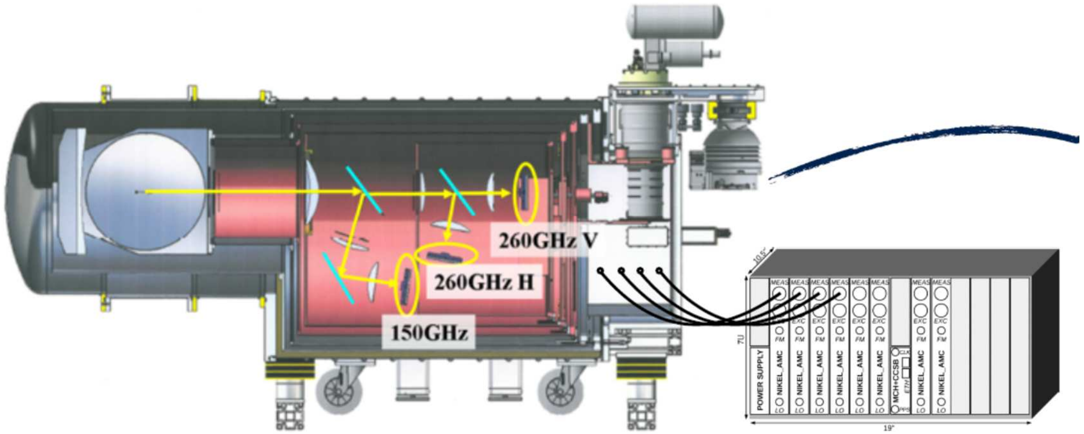

150 GHz - 1 array connected by 4 feed-lines
260 GHz - 2 arrays connected by 8 feed-lines

20 NIKEL readout electronic boxes:
NIKA dedicated readouts, multiplexing factor = 200

NIKA2 main parameters

Frequency	150±20 GHz	260±25 GHz
# KIDs	616 (553)	2 x 1140 (969)
FOV dia	6.5 arcmin	6.5 arcmin
NEFD	8±1 mJy $s^{1/2}$	33±2 mJy $s^{1/2}$
Pixel	17.7±0.1 arcsec	11.2±0.1 arcsec

Adam R., MDP et al. (A&A +18)

Sky positions (in arcsec) of all the validated KIDs for each array

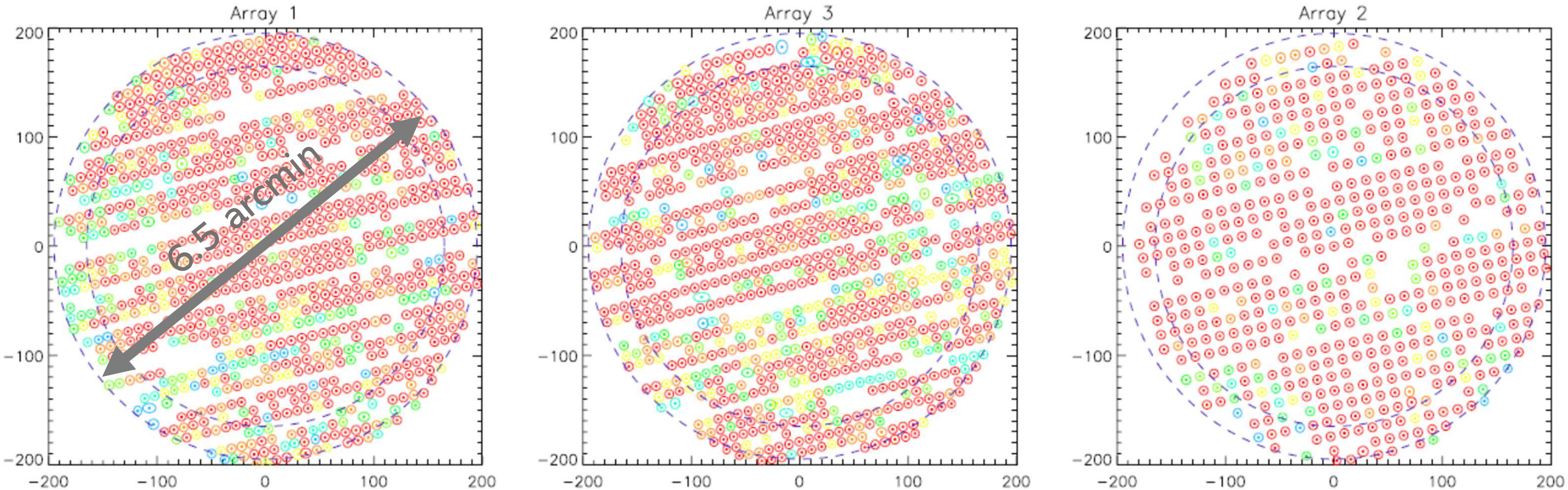

Perotto L., MDP et al. (A&A +20)

NIKA2 @30m IRAM different observation modes

Credits Ruppin F.

Focus

Performing a series of 5 successive one-minute raster scans of a bright (above a few Jy) point source at 5 axial offsets of the secondary mirror (M2) along the optical axis [hourly basis].

The best axial focus is at the maximum of the flux or the minimum of the FWHM.

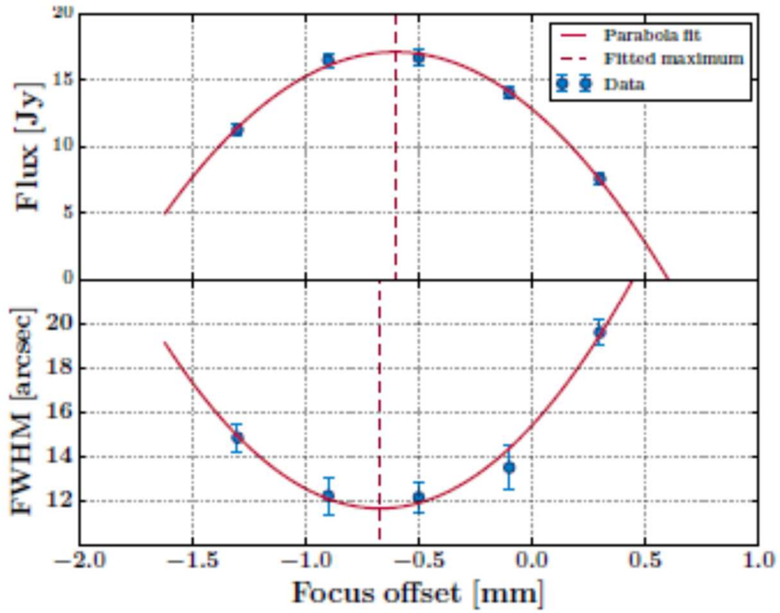

NB the focal plane is not flat but slightly bowl-shaped, …. for this reason it is better to name it focal surface.

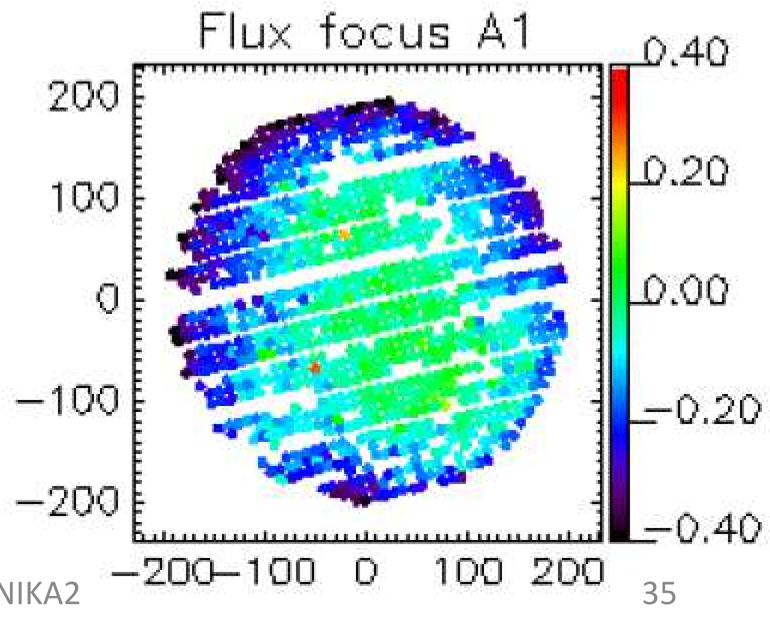

Map of defocus (mm) in Nasmyth offsets (arcseconds)

NIKA2 @30m IRAM different observation modes

Pointing

The telescope executes *back and forth* scan in azimuth and *back and forth* scan in elevation, i.e. a cross-scan, centred on a bright source close to the target one. The estimated position of the reference central detector derives the current pointing offsets of the system in azimuth and elevation [hourly basis]

Credits Ruppin F.

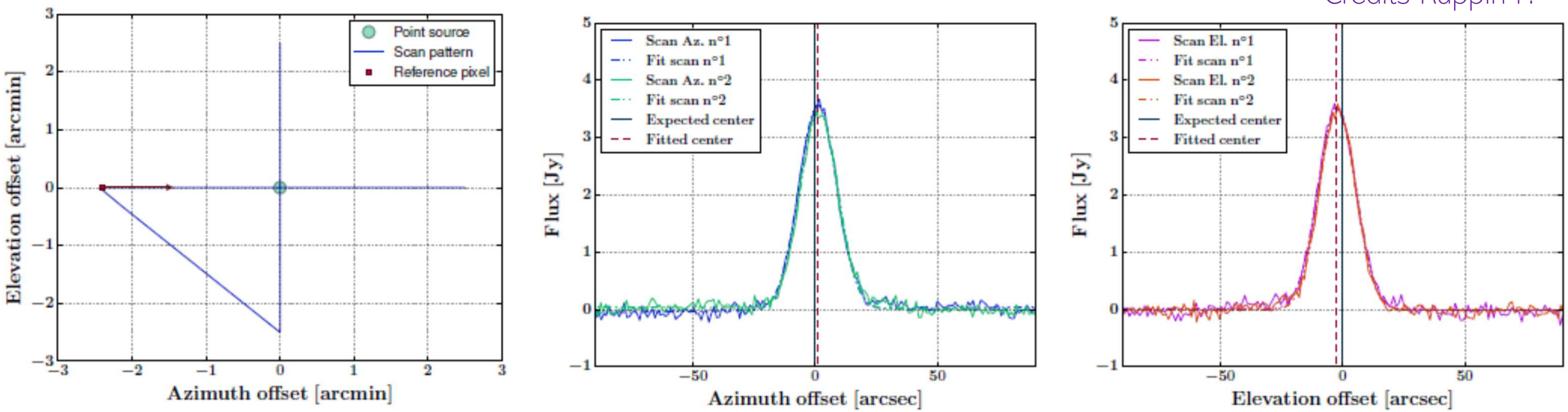

NIKA2@30m IRAM Pointing Session: observing about 30 sources on a wide range of elevations and azimuth angles while monitoring the pointing offsets that are measured for each observation. A corrective model to the coordinates is applied to take into account all the recorded offsets [campaign basis].

NIKA2 @30m IRAM different observation modes

Skydip

A skydip scan consists of a *step-by-step* sky scan along a large range of elevations at fixed azimuth, it comprises 11 steps in the elevation range from 19 to 65 deg, regularly spaced in air mass (~sin(elev)). NIKA2 skydips serve to calibrate the KID responses with respect to the atmospheric background for atmospheric opacity derivation [every eight hours or *shift*].

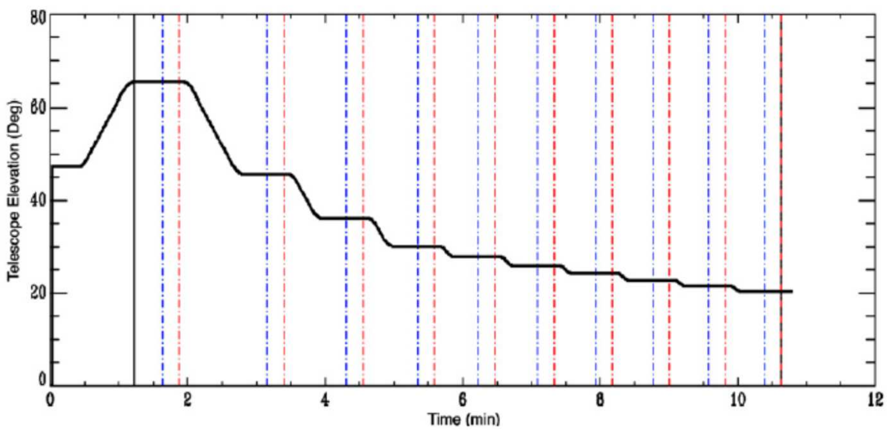

$$f_{\rm reso}^{k} = c_0^k - c_1^k T_{\rm atm}[1 - e^{-\tau_\nu x}]$$

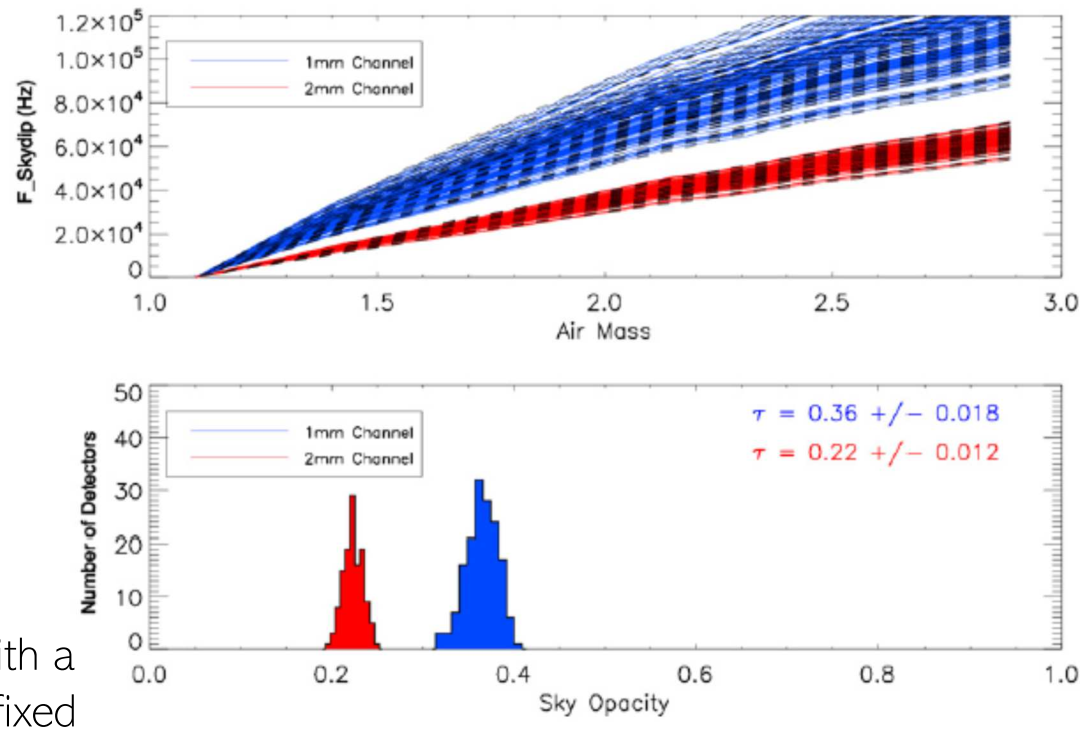

Catalano A. et al. (A&A +14)

The IRAM 30-m telescope facility is also equipped with a resident independent taumeter operating skydips at fixed azimuth every 4 minutes at 225 GHz.

NIKA2 @30m IRAM different observation modes

Beam Map

It is a raster scan in (az; el) to map a bright compact source, often a planet, with steps of 4.8", which are small enough to ensure a half-beam sampling for each KID. A scan of 13 x 7.8 arcmin^2 is acquired. Beammaps are key observations for calibration [daily basis].

OnTheFly maps

Equatorial raster scans on science targets with different orientations (0, +/-45, 90 deg)

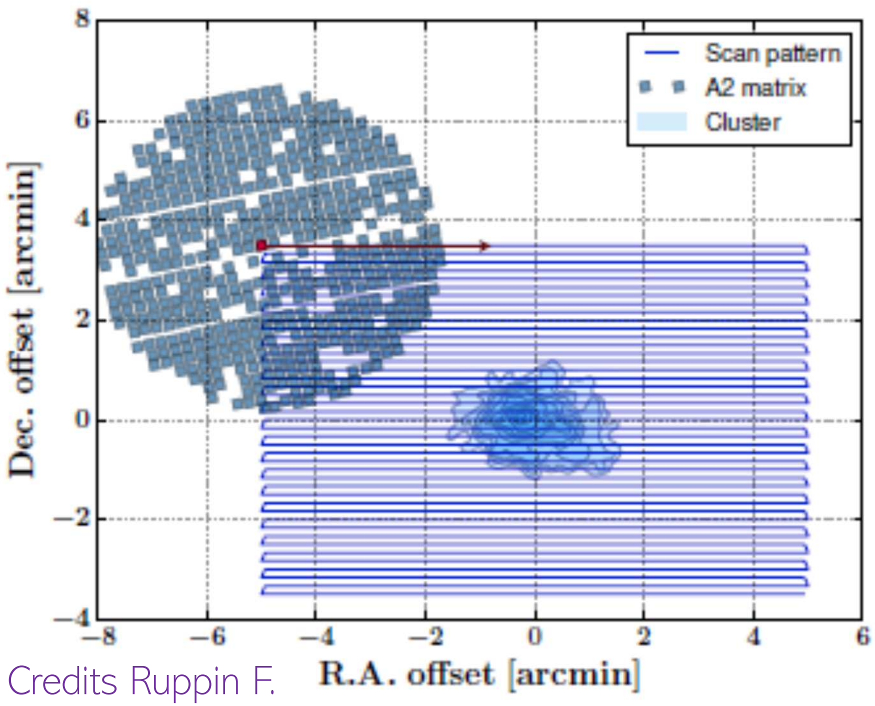

Credits Ruppin F.

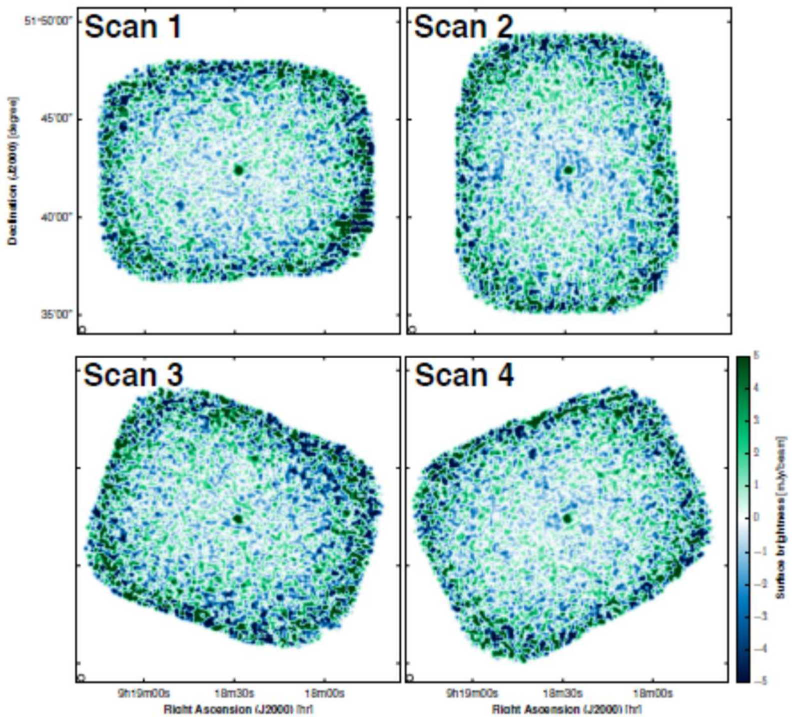

Example of data calibration: Neptune (*i.e.* bright source) scans

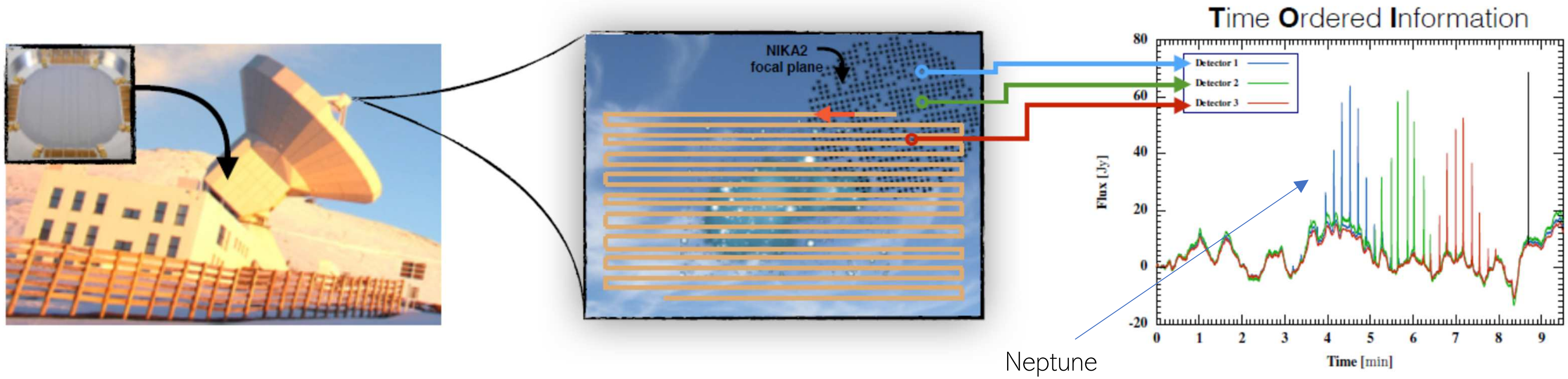

Signal decomposition in the main contributors

Credits Ruppin F.

$$d_k(t) = \underbrace{P_t}_{\text{Pointing matrix}} \times \underbrace{S(\nu, x, y)}_{\text{SZ Signal}} + \underbrace{A(\nu, t)}_{\text{Atmosphere}} + \underbrace{E_k(t)}_{\text{Electronics}} + \underbrace{N_k(t)}_{\text{Detector}} + \underbrace{G_k(t)}_{\text{Glitches}} + \underbrace{C_k(t)}_{\text{Vibrations}}$$

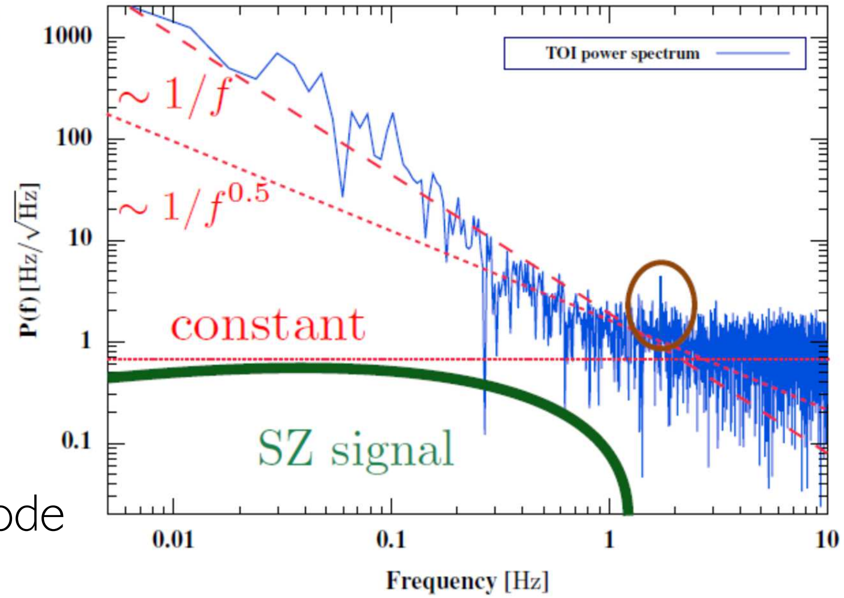

Atmospheric emission is the main contaminant

A dedicated decorrelation method is mandatory:
compromise between residual noise on the map
and signal filtering iterative estimation of the common mode

Summary of the main characteristics describing NIKA2 measured performance

	Array 1 and 3	Array 2
Reference wavelength [mm]	1.15	2.00
Reference frequency [GHz]	260	150
Frequency [GHz]	254.7 and 257.4	150.9
Bandwidth [GHz]	49.2 and 48.0	40.7
Number of designed detectors	1140 and 1140	616
Number of valid detectors [(a)]	952 and 961	553
Fraction of valid detectors [%]	84	90
Pixel size in beam sampling unit [(b)] [λ/D]	1.1	0.87
FWHM [(c)] [arcsec]	11.1 ± 0.2	17.6 ± 0.1
Main beam efficiency [(d)] [%]	47 ± 3	64 ± 3
rms *FWHM* across the FOV [arcsec]	0.6	0.6
Reference FWHM [(e)] [arcsec]	12.5	18.5
Reference beam efficiency [(f)] [%]	61 ± 3	72 ± 2
rms pointing error [arcsec]	<3	<3
Absolute calibration uncertainty [%]	5	5
Systematic calibration uncertainty [(g)] [%]	0.6	0.3
Point-source rms calibration uncertainty [%]	5.7	3.0
α noise integration in time [(h)]	0.5	0.5
NEFD [(i)] [mJy $s^{1/2}$]	30 ± 3	9 ± 1
M_s [(j)] [arcmin^2 mJy^{-2} h^{-1}]	111 ± 11	1388 ± 174

Notes. [(a)]Number of usable detectors, which have been selected in at least two FOV reconstructions. [(b)]Calculated from real array pixel size [2.75 mm/2.0 mm] and unvignetted entrance pupil diameter [27 m]. [(c)]Full width at half maximum of the main beam using the combined results of three methods. [(d)]Ratio between the main beam and the total beam solid angles including large angular-scale error beams and far side lobes. [(e)]Full width at half maximum of the beam used in our reference photometric system. [(f)]Ratio between the reference FWHM beam and the total beam solid angles including large angular-scale error beams and far side lobes. [(g)]Systematic calibration uncertainties due to the opacity correction using the `corrected skydip` method estimated at the reference IRAM 30-m Winter observing conditions: 2 mm pwv, 60° elevation. [(h)]Effective power law of noise reduction with integration time. [(i)]NEFD at zero atmospheric opacity. [(j)]Mapping speed at zero atmospheric opacity.

Perotto L., MDP et al. (A&A +20)

Timescale

- ✓ September 2015: installation at 30m IRAM
- ✓ October 2015: First Light
- ✓ September 2016: complete instrumental setup
- ✓ April 2017: successfully completed commissioning – first science observations
- ✓ October 2017: start public science observations for at least one decade
- ✓ November 2021: 34/45 LP SZ clusters already observed

Collaboration

Involving 150 people in 18 institutes (NIKA2 consortium + IRAM)

NIKA2 @30m IRAM in person and remote observations

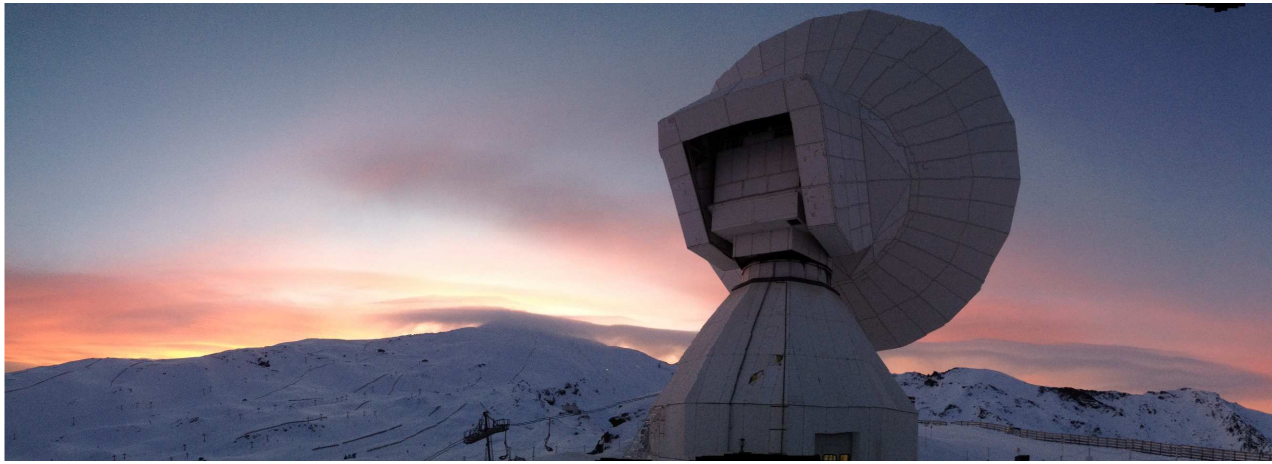

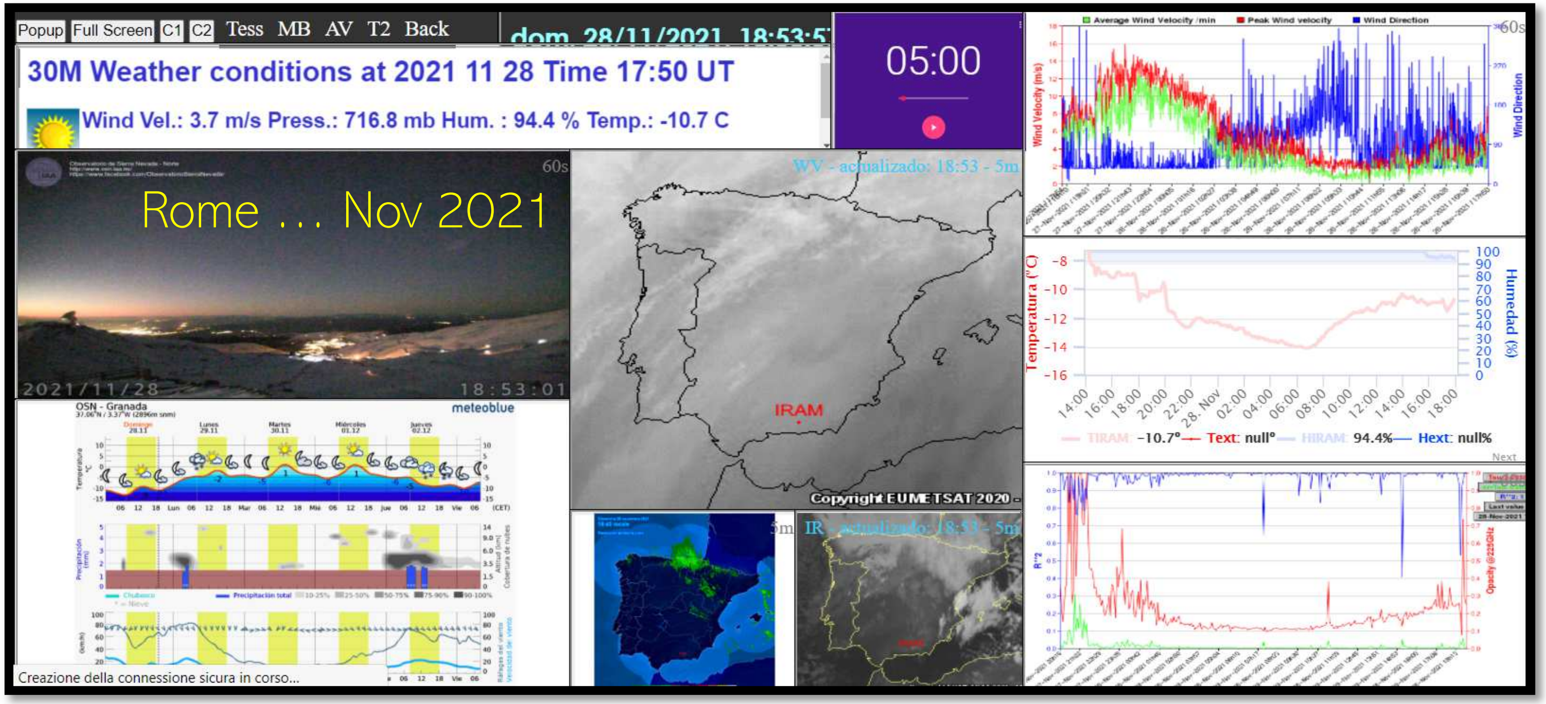

Jamon serrano

LPSZ - Large Program of Sunyaev-Zel'dovich effect

High-resolution mapping of a large sample of high-redshift Galaxy Clusters via SZ effect

- ✓ 300 hours of Guaranteed Time at the IRAM 30-m telescope
- ✓ PI : Frédéric Mayet, coPI : Laurence Perotto (Univ. Grenoble Alpes)
- ✓ 45 clusters at $0.5 < z < 0.9$
- ✓ Follow-up of Planck and ACT (Atacama Cosmology Telescope)
- ✓ Representative: selected in mass and z in the Planck and ACT catalogues
- ✓ X-ray observation available (XMM-Newton and Chandra)
- ✓ + optical follow-ups on-going

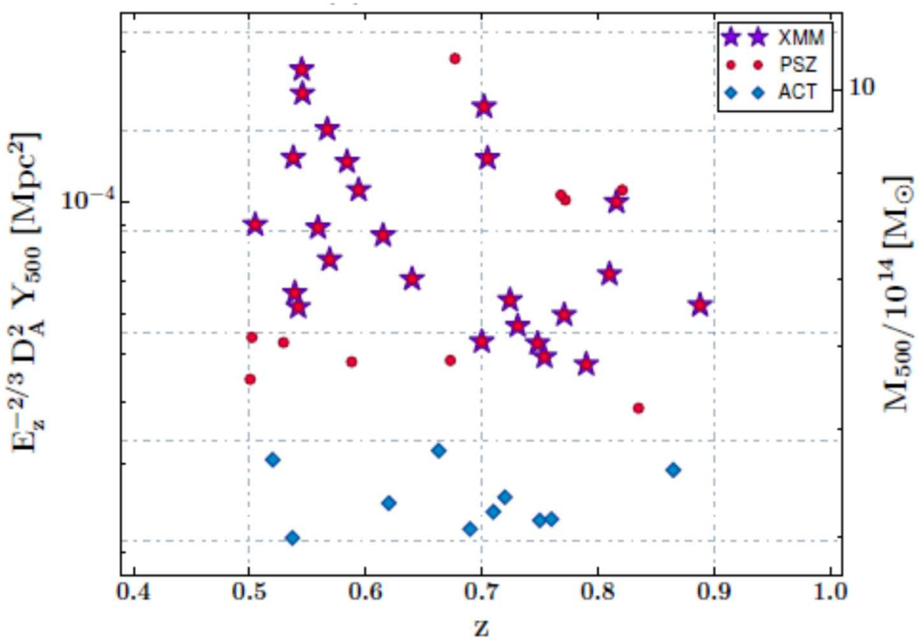

NIKA2 = First generation of SZ experiments for exploiting the synergy between X-rays and SZ at the same angular resolution

PSZ2 G144@

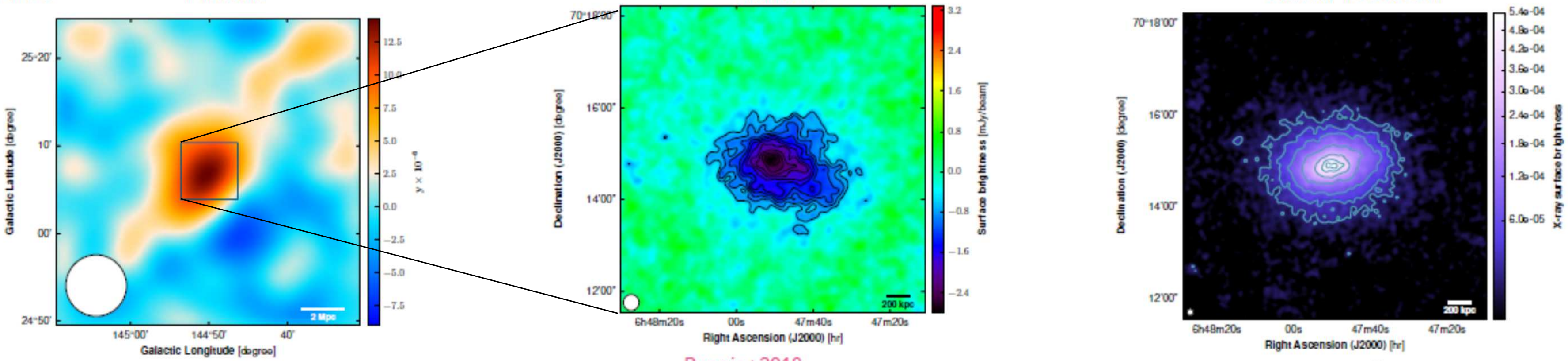

Ruppin+2018

$$\mathcal{D}_A^2\, Y_{500} = 4\pi \frac{\sigma_T}{m_e c^2} \int_0^{R_{500}} r^2 P_e(r)\, dr$$

$$y = \frac{\sigma_T}{m_e c^2} \int P_e(l) dl$$

$$S_X = \frac{1}{(1+z)^4} \int n_e^2(l)\, \Lambda\, dl$$

Deep integration-time spectroscopy $T_e(r)$

Credits Perotto L.

- Full characterization of the Intra-Cluster Medium from the core to the outskirts
- Hydrostatic equilibrium Mass profile from a direct observable of the gas pressure

$$M_{\mathrm{HSE}}(r) \propto \frac{r^2}{n_e(r)} \frac{dP_e(r)}{dr}$$

- Gas temperature profile of high-redshift clusters

$$k_B T_e(r) = \frac{P_e(r)}{n_e(r)}$$

NIKA2 LP-SZ first results: *the demonstrator* PSZ2 G0144

- PSZ2-G0144.83+25.11
- z = 0.58 ; M500 = 7.8x$10^{14}$$M_\odot$
- Science verification, April 2017
- t_obs = 11h
- Atmospheric opacity ≈ 0.3 at 150 GHz
- 13.5 sigma measurement at peak
- tSZ detected up to1.5' (> 0.5 Mpc)

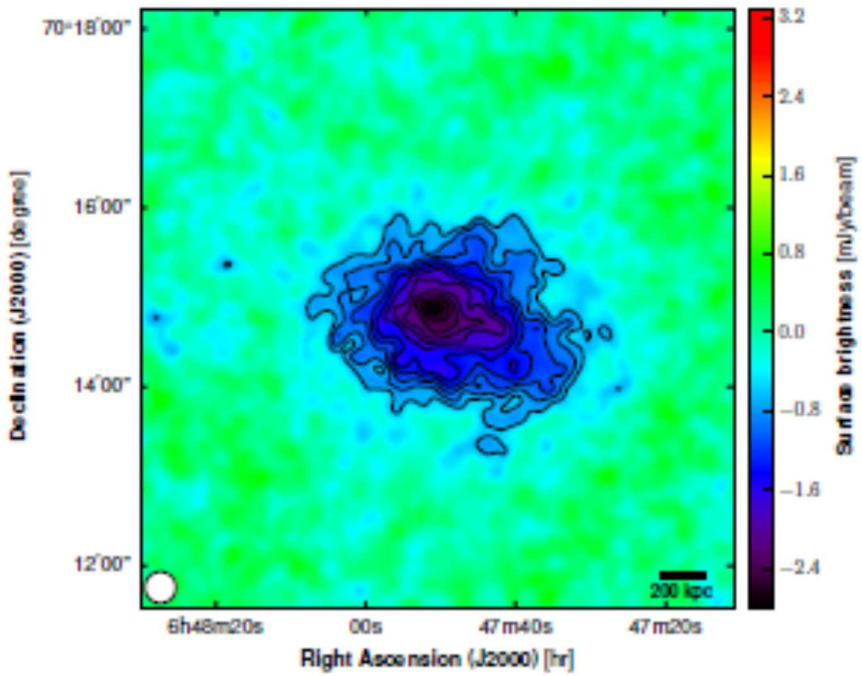

Ruppin F., MDP et al. A&A (2018)

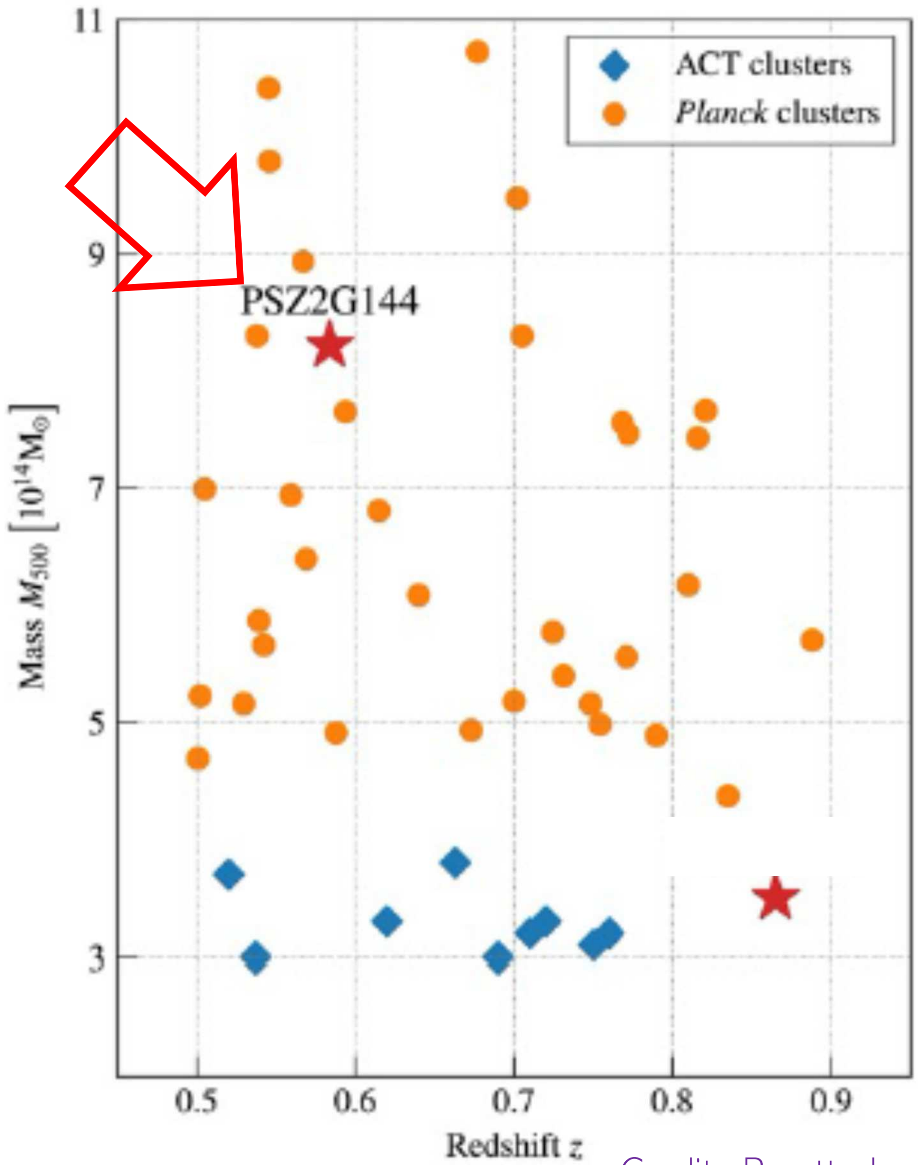

Credits Perotto L.

NIKA2 LP-SZ first results: *the demonstrator* PSZ2 G0144

Implication for the LP-SZ Cosmology Program: **presence of over-pressure regions**

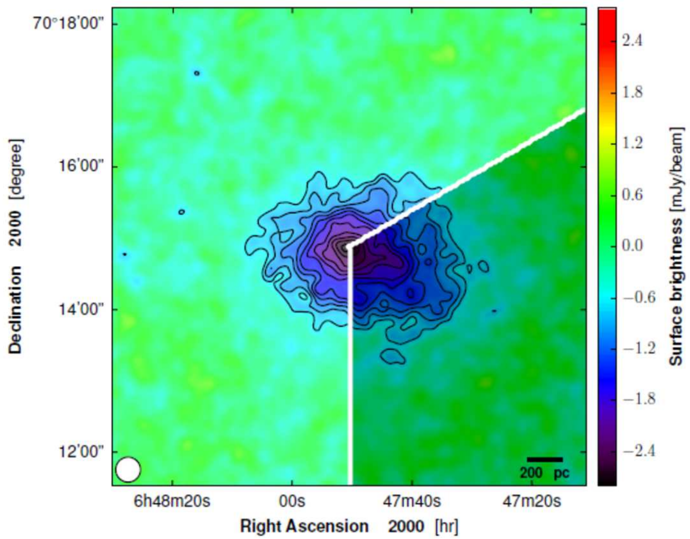

impact on the P-profile

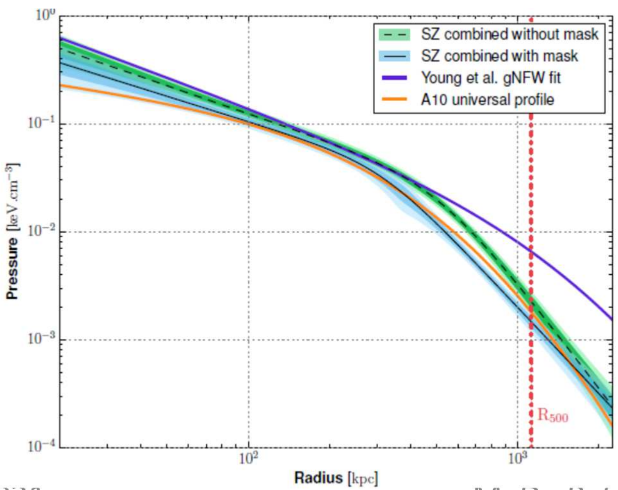

.... and therefore on M and Y

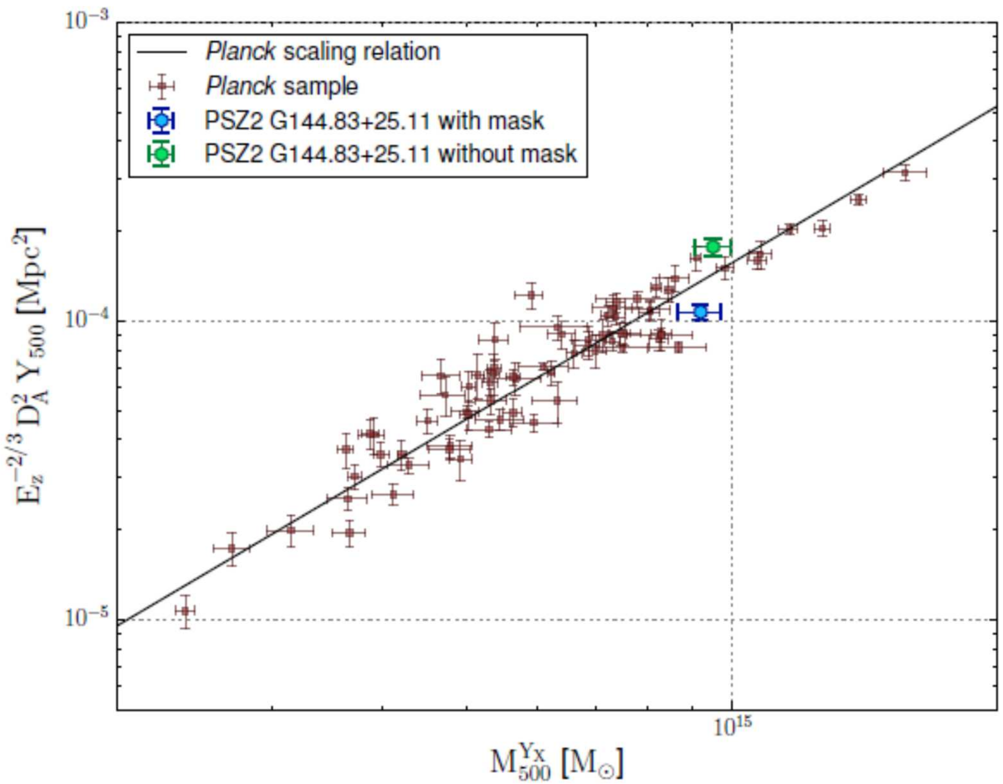

Ruppin F., MDP et al. A&A (2018)

NIKA2 LP-SZ first results: *the challenging* ACT-CL J0215

- ACT-Cl J0215
- $z = 0.865$; $M500 = 3.5 \times 10^{14} M_\odot$
- N2R14, January 2018
- t_obs = 9h
- Atmospheric opacity ≈ 0.2 at 150 GHz
- 9 sigma measurement at peak
- SNR > 3 in a disk of 1 arcmin square

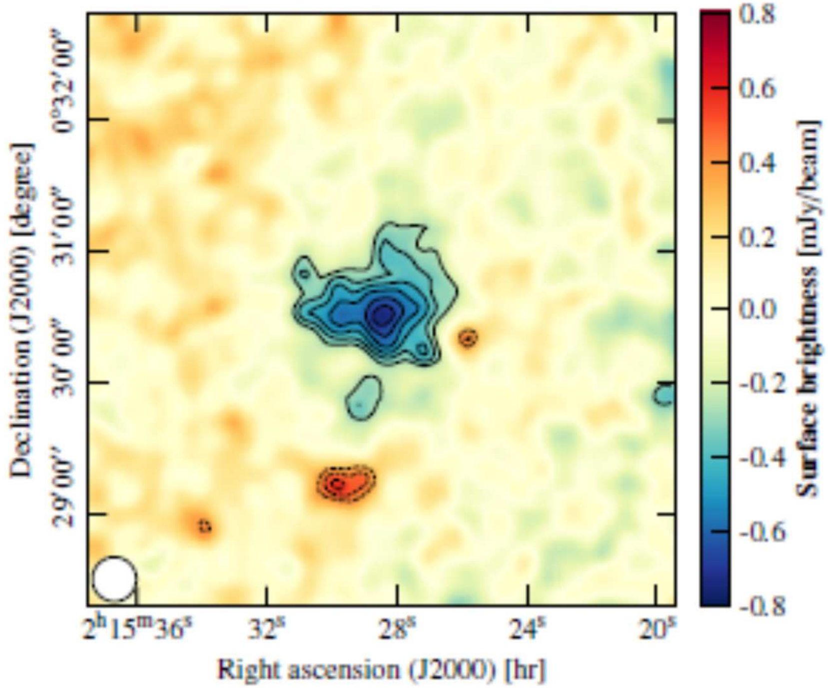

Kéruzoré F., MDP, et al. A&A (2020)

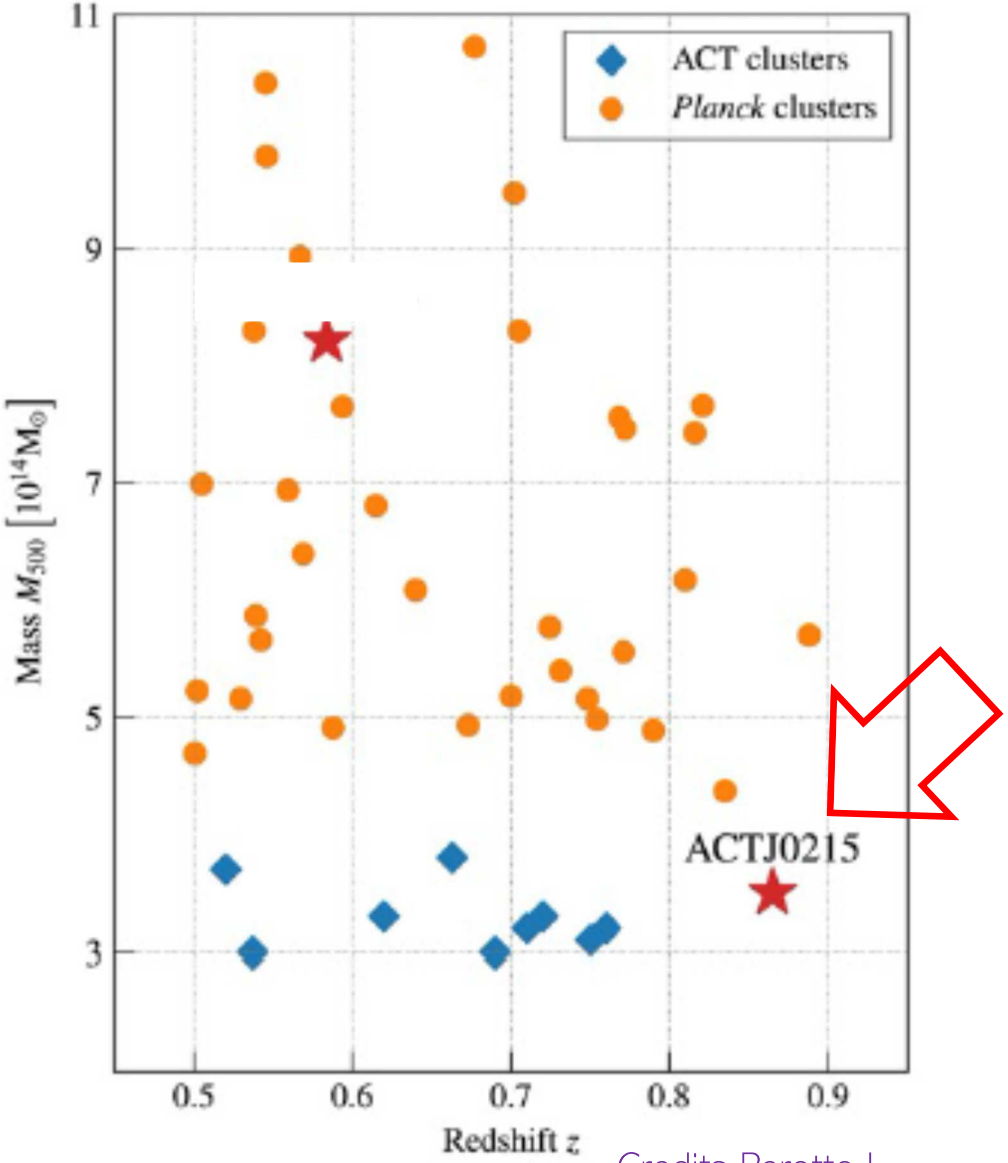

Credits Perotto L.

NIKA2 LP-SZ first results: *the challenging* ACT-CL J0215

Implication for the LP-SZ Cosmology Program: **impact of point sources**

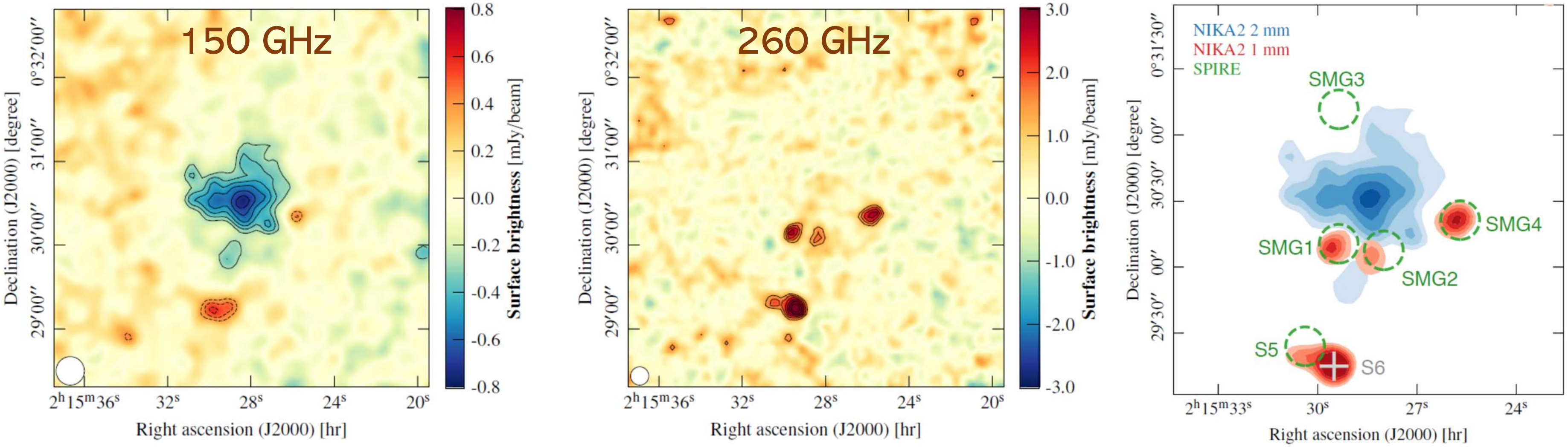

Kéruzoré F., MDP, et al. A&A (2020)

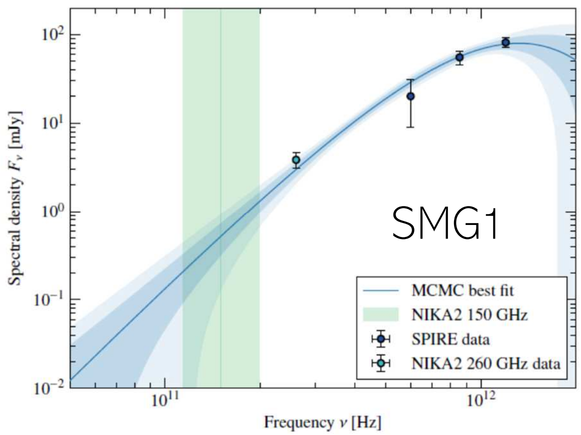

Fit of the **point source flux** in the 150 GHz band from NIKA2@260GHz + SPIRE@600, 800, 1200 GHz

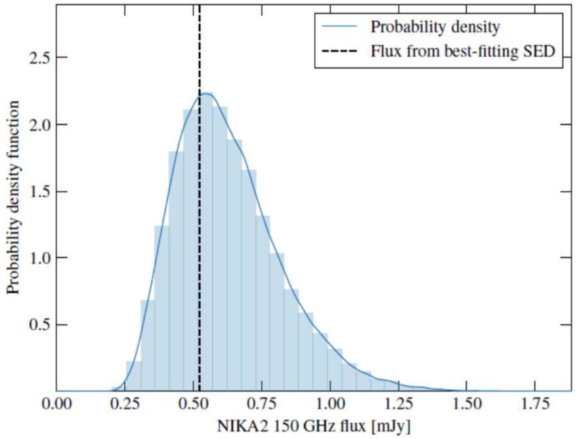

Probability distribution of the point source flux at 150 GHz

NIKA2 LP-SZ first results: *the challenging* ACT-CL J0215

Implication for the LP-SZ Cosmology Program: **impact of point sources**

Pressure profile with NIKA2+ACT

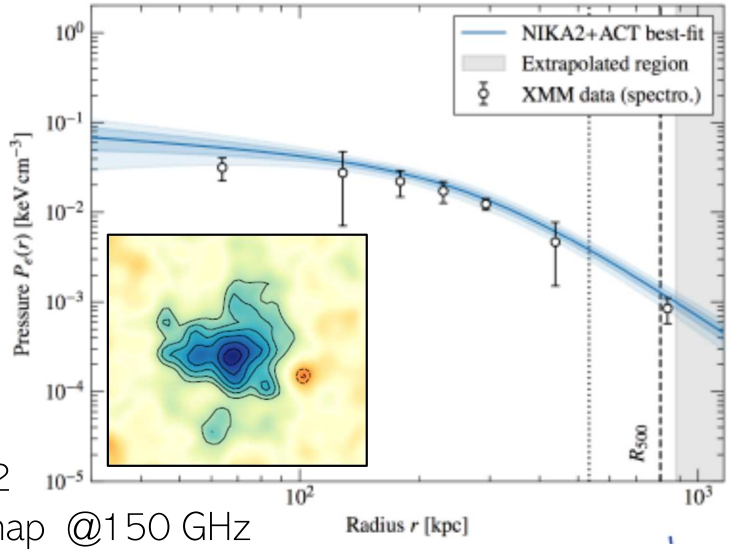

NIKA2 tSZ map @150 GHz

+

Density profile with XXM-Newton

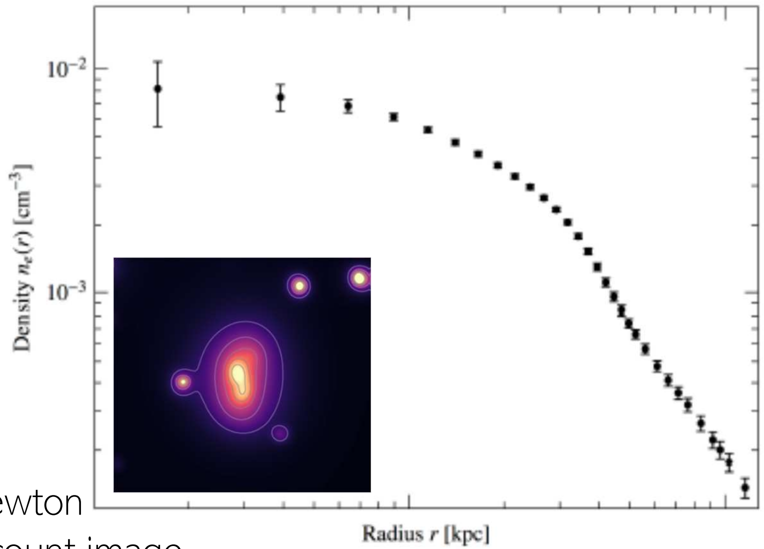

XMM-Newton photon-count image

Kéruzoré F., MDP, et al. A&A (2020)

	ACT	XMM-*Newton*	NIKA2+XMM
R_{500} [kpc]	877.8 ± 46.2	780.9 ± 19.8	810.1 ± 41.9
$\mathcal{D}_A^2\, Y_{500}$ [10^{-5} Mpc^2]	4.07 ± 1.13	–	3.76 ± 0.39
M_{500} [10^{14} M$_\odot$]	3.5 ± 0.8	2.48 ± 0.70	3.79 ± 0.58

Precision improvement on **Y500** w.r.t.
- ACT

Precision improvement on **M500** w.r.t.
- ACT (using Y-M scaling law) and
- XMM-Newton (alone)

NIKA2 LP-SZ first results: *the challenging* ACT-CL J0215

Implication for the LP-SZ Cosmology Program: **ICM radial profiles**

Imaging synergy among NIKA2, ACT, XMM-Newton and Herschel (follow-up with NOEMA)

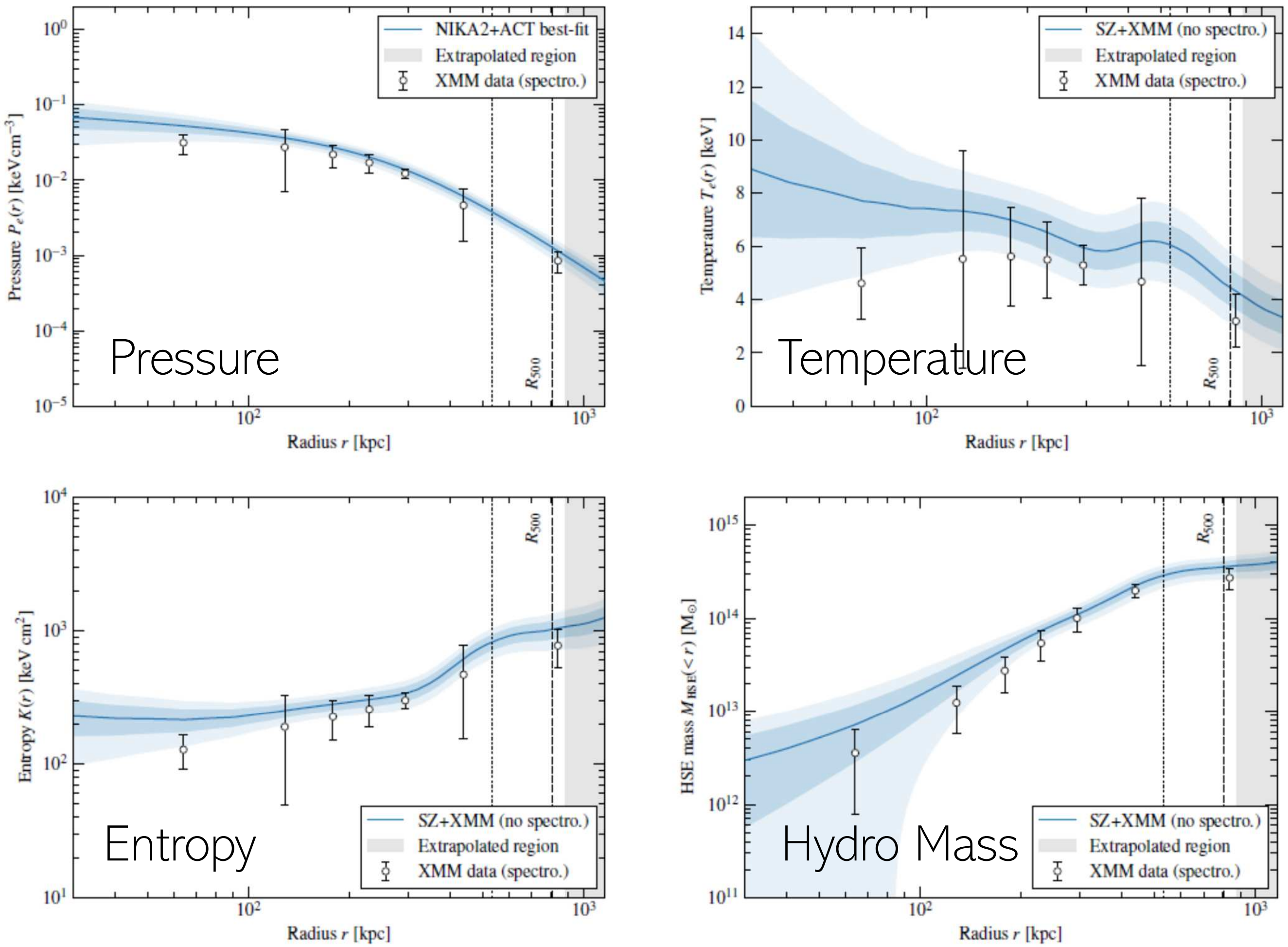

Take home message:
even if this cluster is distant with low mass and is a disturbed cluster, NIKA2 obs improved:

1- the precision of the mass (M_{500}=3.79±0.58 $10^{14} M_\odot$) and

2- the knowledge of the thermodynamical properties obtained from the combination of NIKA2 and XMM-Newton, very competitive with those obtained using X-ray spectroscopy (obs time expensive).

NIKA2 LP-SZ current status

Status of the observation of the cluster sample L. Perotto et al. EPJ submitted

45 clusters in total

- 31 already observed
- 3 started
- 7 scheduled (including 4 ACT clusters)
- 4 not a cluster (to change)

1. Point source detection and removal
2. Estimation of the thermodynamical profiles: Pressure, Temperature, HSE Mass
3. Statistical analysis tools for Cosmology

NIKA2 LP-SZ current status

Status of the observation of the cluster sample L. Perotto et al. EPJ submitted

45 clusters in total

- 31 already observed
- 3 started
- 7 scheduled (including 4 ACT clusters)
- 4 not a cluster (to change)

1. Point source detection and removal
2. Estimation of the thermodynamical profiles: Pressure, Temperature, HSE Mass
3. Statistical analysis tools for Cosmology

MUSIC Twin Sample (Marenostrum MUltidark SImulations of galaxy Clusters)

Sembolini F. MDP et al. (2013)

MUSIC-2 : resimulated clusters from MultiDark Simulation, a DM only N-body simulation with 2048^3 dark matter particles in a 1 h^{-1} Gpc cubic box

- >500 clusters $M>10^{14}h^{-1}M_\odot$
- >2000 clusters $M>10^{13}h^{-1}M_\odot$

with radiative physics (CSF, *i.e.* cooling + SFR + UV photoionization + SN feedbacks), non radiative (NR) and with AGN.

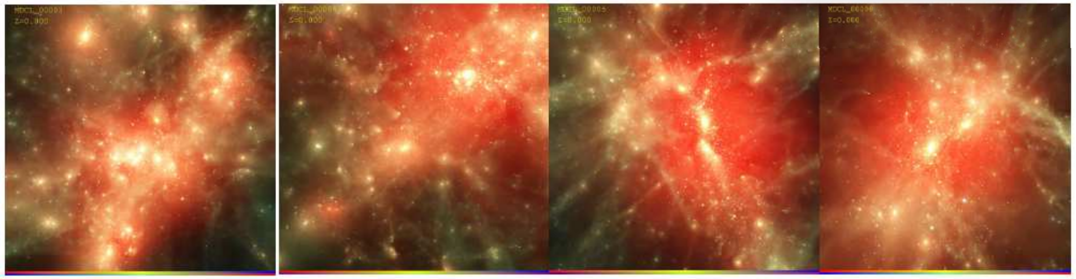

4 MUSIC clusters with radiative physics (CSF) at z=0

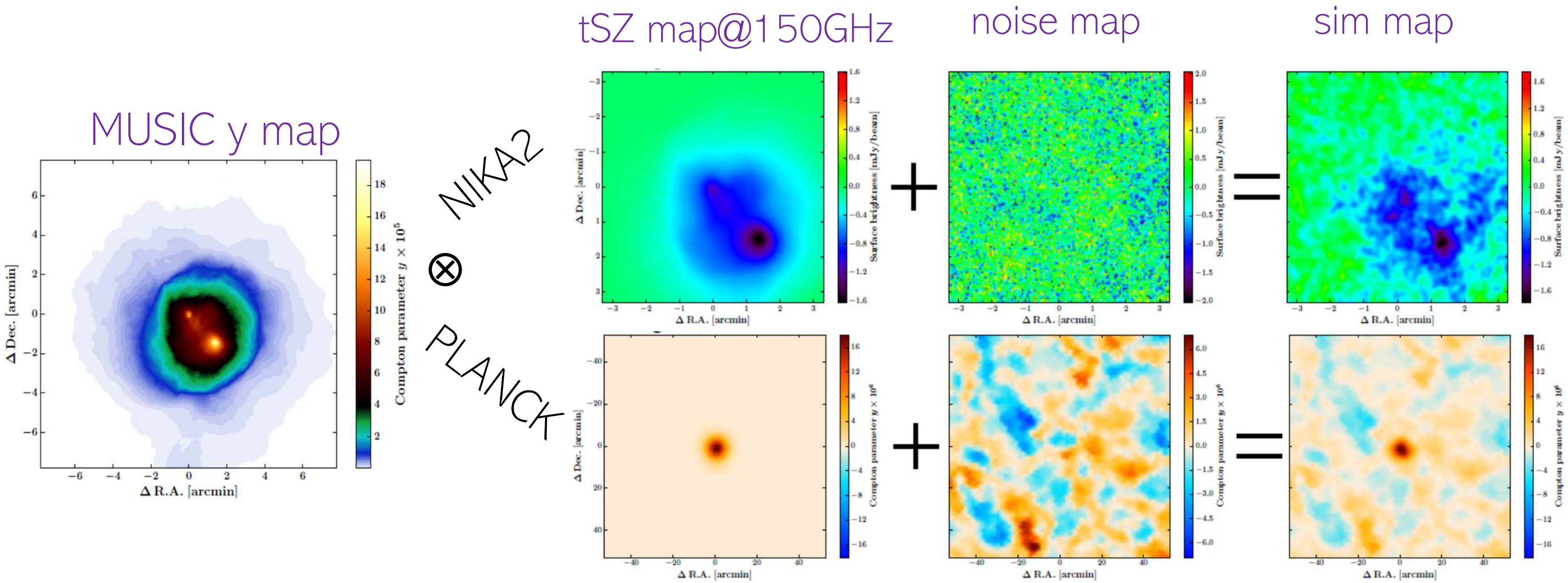

Ruppin F., MDP et al. (2019)

MUSIC Twin Sample (Marenostrum MUltidark SImulations of galaxy Clusters)

Sembolini F. MDP et al. (2013)

tSZ mock images of NIKA2 Twin Sample extracted from MUSIC synthetic clusters useful to check the impact of dyamical state (i.e. morphology) on pressure profiles recovery.

tSZ maps at 150 GHz at 20" resolution for relaxed and disturbed clusters

radial pressure profiles: NIKA2 and Planck mock images and MUSIC data

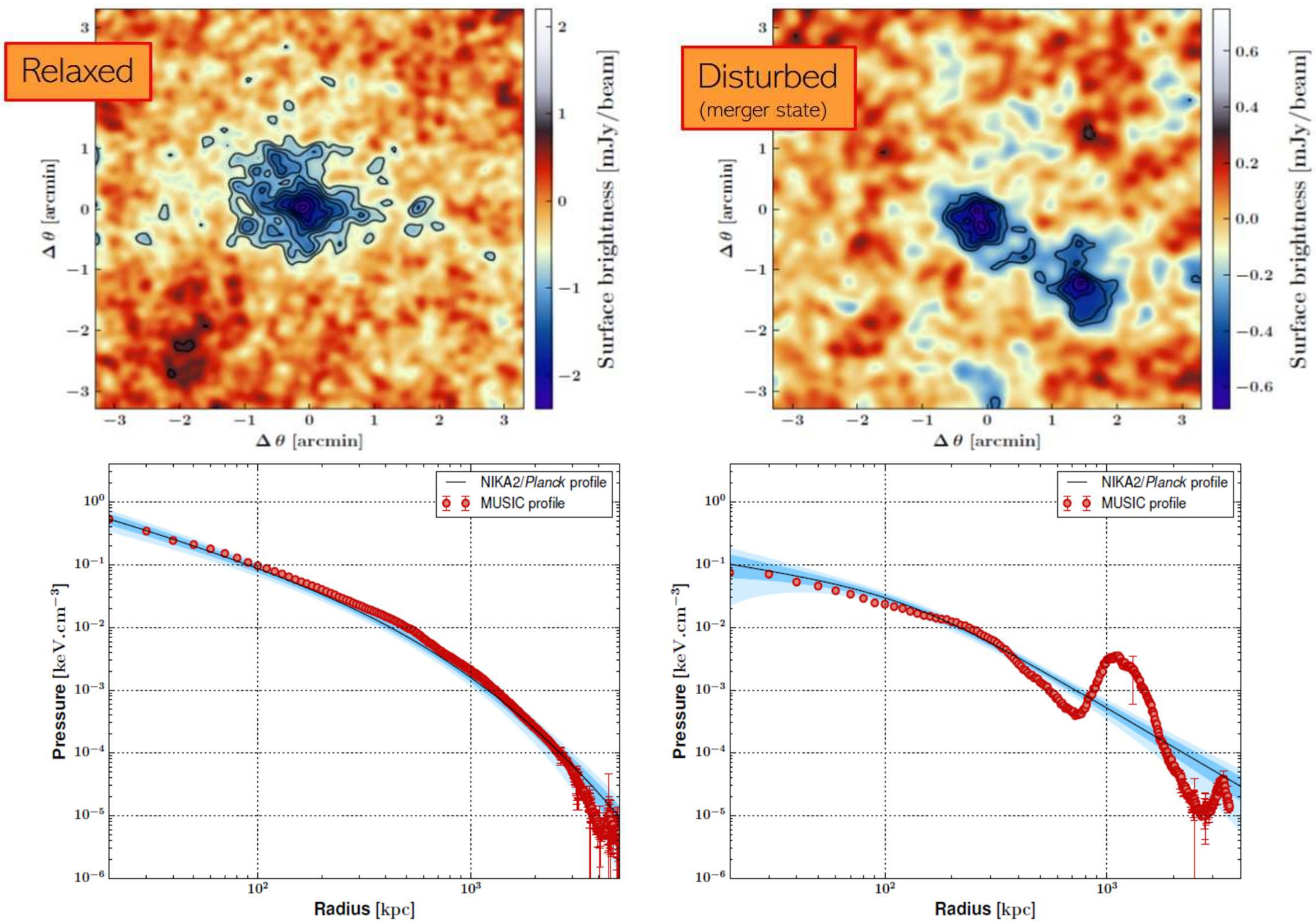

Ruppin F., MDP et al. (2019)

Modeling Galaxy Clusters and their environment

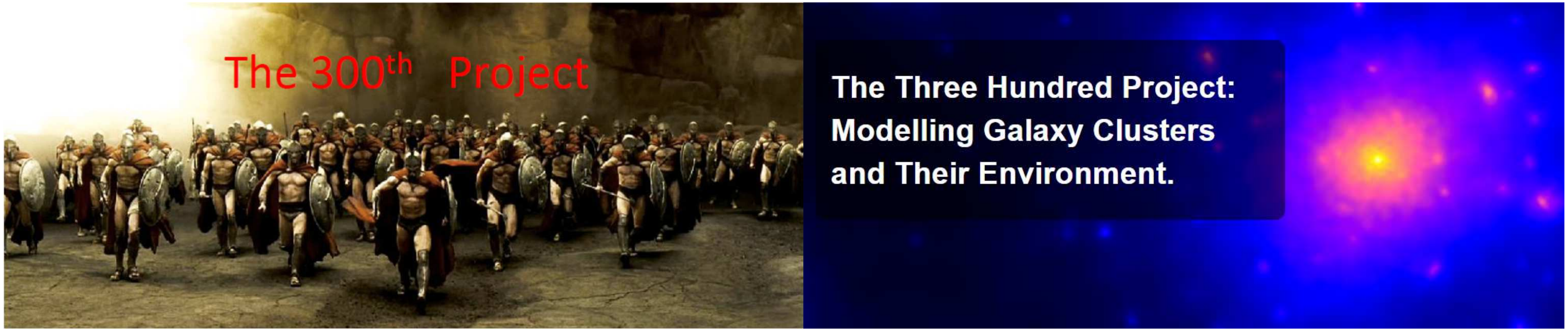

https://www.nottingham.ac.uk/~ppzfrp/The300/people.php Cui W. MDP et al. (2018)

- 300+ Clusters selected from a new Multidark Planck 1Gpc volume done in Planck cosmology.
- Larger resimulated areas (15 Mpc radius) .
- Several SPH, AMR and Moving Mesh codes + different subgrid physics implementations.
- Synthetic maps of X-ray, SZ, Optical and Lensing will be provided to user participants.
- Re-simulation of 324 large galaxy clusters with full-physics hydrodynamical re-simulations.
- All simulations and derived data products are publicly available

The300 Twin Samples (The Three Hundred project)

Cui W. MDP et al. (2018)

3 twin samples: 1) total mass (TS_{TM}), hydrodynamic mass (TS_{HEM}), and integrated Compton parameter at R500 (TS_{Y}).

For each TS we have mock observations in X-ray, SZ, Optical, lensing of LPSZ

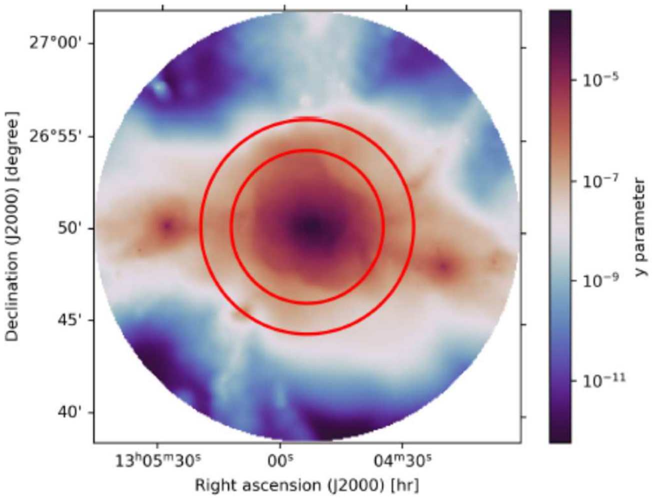

Compton parameter map

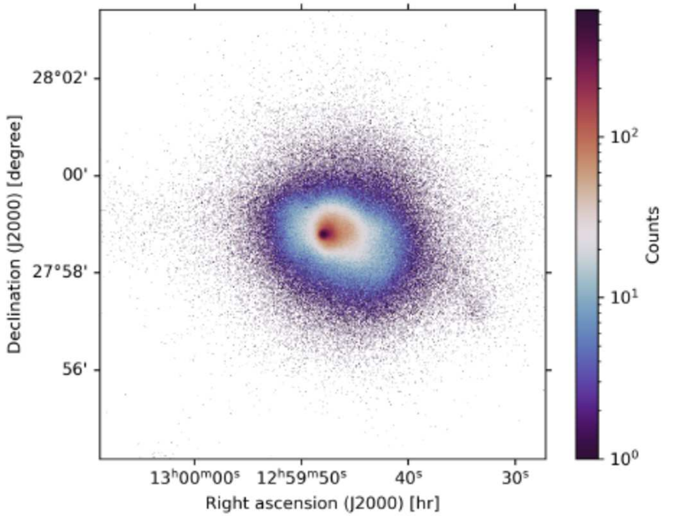

Mock X-Ray photon count image for the Athena Wide Field Imager

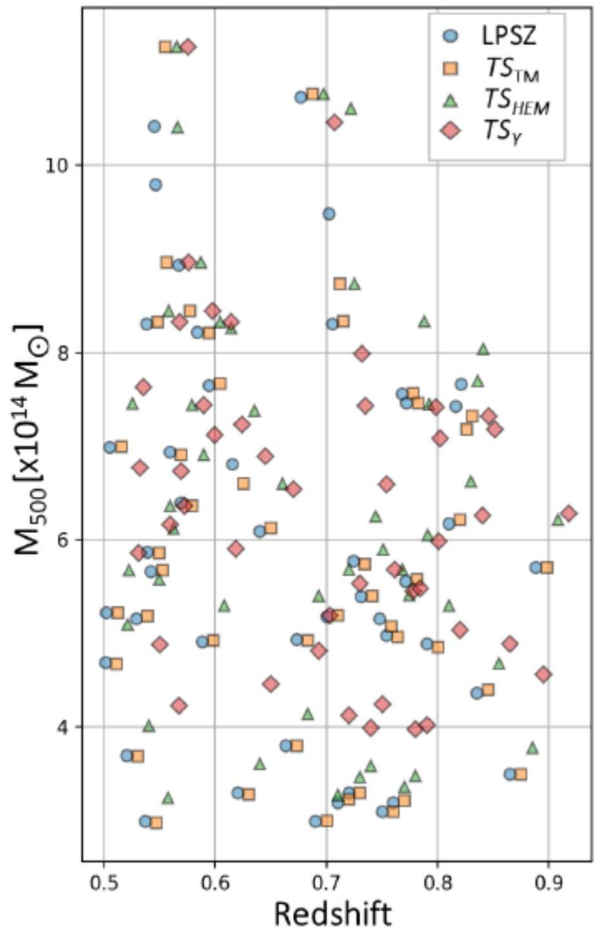

A. Paliwal et al. EPJ submitted

- Test novel methods on realistic simulation, assess the impact of dynamical state, z-evolution
- Forecast NIKA2 LP-SZ uncertainties on scaling laws and biases and capability to measure f_{gas}, H_0

R. Adam, P. Ade, N. Aghanim, P. André, M. Arnaud, H. Aussel, R. Barrena Delgado, I. Bartalucci, A. Beelen, A. Benoît, A. Bideaud, N. Billot, O. Bourrion, M. Calvo, A. Catalano, N. Clerc, G. Coiffard, B. Comis, M. De Petris, F.-X. Désert, M. Douspis, S. Doyle, C. Ferrari, J. Goupy, C. Kramer, G. Lagache, S. Leclercq, J.-F. Lestrade, J.F. Macías-Pérez, P. Mauskopf, F. Mayet, J.-B. Melin, A. Monfardini, E. Pascale, L. Perotto, G. Pisano, E. Pointecouteau, N. Ponthieu, G. Pratt, V. Revéret, A. Ritacco, C. Romero, H. Roussel, J. A. Rubino Martin, F. Ruppin, K. Schuster, A. Sievers, S. Triqueneaux, C. Tucker, R. Zylka

Bibliography

- Adam R., MDP, et al. A&A 609, A115 (2018)
- Baars J.W.M., et al., A&A 175, 319 (1987)
- Calvo, M., et al. 2016, J. Low Temp. Phys., 184, 816
- Capalbo V. MDP et al. MNRAS 503, 6155–6169 (2021)
- Catalano A. et al. A&A 569, A9 (2014)
- Cialone G., MDP et al. MNRAS 477, 139–152 (2018)
- Cui W., MDP, et al. MNRAS 480, 2898–2915 (2018)
- De Luca F., MDP et al. MNRAS 504, 5383–5400 (2021)
- Gianfagna G., MDP, et al. MNRAS 502, 5115–5133 (2021)
- Kaiser, N., MNRAS, 222, 323 (1986)
- Kéruzoré F., MDP et al. A&A 644, A93 (2020)
- Mroczkowski T. et al. Space Sci Rev 215:17 (2019)
- Nagai D. et al. ApJ, 668:1-14, (2007)
- Paliwal A. MDP et al. mm Universe @NIKA2 proceedings, EPJ submitted
- Pardo J. R., et al., IEEE Trans. Antennas Propagation, 49, 1683 (2001)
- Perotto L., MDP, et al. A&A 637, A71 (2020)
- Perotto L. MDP et al., mm Universe @NIKA2 proceedings, EPJ submitted
- Planck 2013 results. XX. A&A 571, A20 (2014)
- Planck 2015 results. XXIV A&A 594, A24 (2016)

Bibliography

- Roesch, M., et al., 2012, ISSTT2011 Workshop [arXiv:1212.4585]
- Ruppin F., MDP et al. A&A 615 A112 (2018)
- Ruppin F. MDP et al., A&A 631, A21 (2019)
- Salvati L. et al. A&A 614, A13 (2018)
- Salvati L. et al. A&A 626, A27 (2019)
- Sembolini F. MDP et al. MNRAS 429, 323–343 (2013)
- Sunyaev R.A. and Zel'dovich Y.B., Comm. A.S.P., 4, 173, (1972)
- Voit, G. M., Rev. Mod. Phys., 77, 207 (2005)
- Zel'dovich Y.B. and Sunyaev R.A., Astrophys. Space Sci. 4, 301 (1969)

Useful links

- NIKA2 https://ipag.osug.fr/nika2//Welcome.html
- IRAM https://www.iram-institute.org/
- LPSZ NIKA2 http://lpsc.in2p3.fr/NIKA2LPSZ/

Questions?

Do you need more information?

Contact: Marco De Petris
marco.depetris@uniroma1.it
Sapienza University - Dept. of Physics
Marconi Building, room n° 152, 1st floor - ☎ +39-06-49914690